Study of phase-separation dynamics by use of cell dynamical systems. II. Two-dimensional demonstrations

S. Puri and Y. Oono
Department of Physics and Materials Research Laboratory, 1110 W. Green Street, University of Illinois–Urbana-Champaign, Urbana, Illinois 61801

(Received 9 November 1987; revised manuscript received 18 March 1988)

We present detailed results on the form factors of two-dimensional systems undergoing phase-ordering processes, using both deterministic and stochastic cell dynamical systems. We show the robustness of the asymptotic form factors against quench depth, noise amplitude, etc. The effect of noise is essentially to delay the number of steps needed to reach the asymptotic behavior. In the case with a nonconserved order parameter, we demonstrate that the form factor obtained by T. Ohta, D. Jasnow, and K. Kawasaki [Phys. Rev. Lett. **49**, 1223 (1982)] is asymptotically very accurate. We also present preliminary results for off-critical quenches.

I. INTRODUCTION

In contrast to the dynamics of second-order phase transitions, the dynamical aspects of first-order phase transitions are not yet very well understood. A classic representative problem in this field is the ordering kinetics of thermodynamically unstable phases, e.g., spinodal decomposition.[1] Many experimental,[2,3] numerical,[4–8] and analytical[9–13] approaches have been applied to this problem.

Numerical approaches include Monte Carlo simulations[4–6] and simulations of phenomenological (stochastic) partial differential equations (PDE's).[7] These numerical simulations are useful but suffer from present day computational limitations which impose the following restrictions: (a) it is difficult to study the long-time behavior of the ordering process (e.g., the so-called scaling regime in spinodal decomposition); (b) to date, there have been no numerical studies of the effect of hydrodynamics on the separation process. This is due to the long-range nature of hydrodynamic interactions which requires a huge system for an accurate simulation. Analytical approaches have the problem that the process of phase separation is highly nonlinear. Thus, especially for long-time behaviors, the approximations used in analytical theories have not been mathematically well controlled.

This paper is the second part of a two-part exposition. Our first paper[14] (henceforth called part I) proposed a cell-dynamical-system (CDS) approach to phase-ordering dynamics[15] and provided a detailed methodological account. In that paper, we studied the general features of our approach but we confined ourselves to deterministic models. In this paper, we present detailed results from our study (using these CDS models) of phase-ordering dynamics in two-dimensional isotropic systems with a scalar order parameter and without hydrodynamic interactions. Here, we make a detailed comparison of results from both deterministic and stochastic models. We focus our attention on form factors, and show that the deterministic model and the stochastic model give indistinguishable form factors. In the nonconserved-order-parameter case, the effect of the finite interface thickness on the form factor is analytically studied, and the comparison of this and our CDS results strongly suggests that the form factor given by Ohta, Jasnow, and Kawasaki (OJK) [Ref. 11 (b)] is very accurate, if not exact.

This paper is organized as follows. In Sec. II, we briefly survey relevant results (experimental and numerical) in this field. In Sec. III, we summarize our CDS models (without and with noise). In Sec. IV, we present detailed results for the case with a nonconserved order parameter. In Sec. V, we present detailed results for the case with a conserved order parameter under the condition of a "critical quench." Preliminary results for the case of a conserved order parameter with an "off-critical quench" are presented in Sec. VI. Section VII is devoted to a discussion and summary of this paper.

II. BRIEF SUMMARY OF EXPERIMENTAL AND NUMERICAL RESULTS

As already stated in the Introduction, we consider only systems with scalar order parameters without hydrodynamics. The mechanisms whereby ordering takes place in such systems depends crucially on whether the order parameter is nonconserved or conserved. In almost all analytical approaches the starting point is a stochastic PDE,

$$\frac{\partial\psi(\mathbf{r},t)}{\partial t}=-L(i\nabla)^{2\beta}\frac{\delta H[\psi(\mathbf{r},t)]}{\delta\psi(\mathbf{r},t)}+\sigma(\mathbf{r},t)\ , \tag{2.1}$$

where $\psi(\mathbf{r},t)$ is the order parameter of the system at point $\mathbf{r}$ at time t; L is a phenomenological parameter; $\beta=1$ for the conserved-order-parameter case [called the Cahn-Hilliard-Cook (CHC) equation[9]] and $\beta=0$ for the nonconserved case [called the time-dependent Ginzburg-Landau (TDGL) equation]; $H[\psi(\mathbf{r},t)]$ is usually the coarse-grained ϕ^4 free-energy functional

$$H[\psi(\mathbf{r},t)]=\int d\mathbf{r}\left[\tfrac{1}{2}(\nabla\psi)^2-\frac{\tau}{2}\psi^2+\frac{g}{4}\psi^4\right]\ , \tag{2.2}$$

with τ,g being phenomenological parameters greater than

zero. The parameter τ measures the depth of the quench. The Gaussian white noise $\sigma(\mathbf{r},t)$ has the following expectation values:

$$\langle \sigma(\mathbf{r},t)\rangle = 0 ,$$
$$\langle \sigma(\mathbf{r},t)\sigma(\mathbf{r}',t')\rangle = 2L(i\nabla)^{2\beta}\delta(\mathbf{r}-\mathbf{r}')\delta(t-t') . \quad (2.3)$$

In the conserved-order-parameter case, $\int d\mathbf{r}\,\psi(\mathbf{r},t)$ is a constant. If this constant is zero, we say that the quenching is critical. If this constant is nonzero, the quenching is said to be off-critical.

Recent interest in the study of phase-ordering dynamics is due to the observation of an approximate scaling law in Monte Carlo simulations.[4,5] These suggested that the normalized form factor $S(\mathbf{k},t)$ has a scaling regime in which it behaves as

$$S(\mathbf{k},t) = l(t)^d \Phi(kl(t)) , \quad (2.4)$$

where $\mathbf{k}$ is the wave vector; t is the time; Φ is a universal function; $l(t)$ is a time-dependent length scale (interpreted as the typical domain size) which behaves as $l(t)\sim(t-t_0)^{\phi}$ for some positive number ϕ, t_0 being a "starting time"; and d is the spatial dimensionality. It should be noted that, previous to these results, Binder and Stauffer[10(a)] and Furukawa[10(b)] had discussed possible scaling of the form factor.

Experimental studies on a number of different systems have found the approximate scaling as described by (2.4) and also the power-law growth law for the representative domain size. For the case when the order parameter is not conserved, the power-law growth rate with $\phi\sim 0.5$ [called the Lifshitz-Cahn-Allen (LCA) growth law] has been observed in a variety of experimental situations.[2] As far as we are aware, Noda *et al.*[2(c)] were the first to demonstrate (experimentally) the scaling of the form factor in the nonconserved case.

In the absence of hydrodynamics, the phase-separation process with a conserved order parameter has been studied by a number of different groups.[3] In a recent letter, Gaulin *et al.*[3(b)] reported results from their studies of phase segregation in critically quenched samples of $Mn_{0.67}Cu_{0.33}$. They observed a late-time regime in which the form factors scaled well with an exponent $\phi\sim 0.33$. Prior to this regime, they saw a power-law growth with a smaller effective exponent. These experimental results suggest that different mechanisms (and combinations of them) are responsible for domain growth in different time regimes.

There are a number of numerical simulations of the process. These are all without hydrodynamic interactions. The nonconserved case was studied by Phani *et al.* and others[4] via Monte Carlo simulations. They found that dynamical scaling was satisfied and obtained the form of Φ. The result for the exponent ϕ is compatible with the LCA value of $\phi\sim\frac{1}{2}$. For the conserved case, extensive Monte Carlo simulations (using a spin-exchange kinetic Ising model) were performed by Marro *et al.*[5] They found that ϕ varies between 0.19 and 0.3 depending on the depth of quenching, the off criticality, and the time of evolution. As in the experimental case, there was an approximate scaling in the sense that data for fairly long periods of time could be fitted to master curves. However, they found that the shape of the master curve changed gradually in time so that data for very long time periods could not be fitted to a single curve. Another Monte Carlo study of the conserved case was done by Mazenko *et al.*,[6(a)] who used a renormalization-group method to extract the domain growth law. They originally claimed a logarithmic growth rate asymptotically, at variance with all other results. Huse[6(b)] criticized these results and his Monte Carlo results for the conserved case found (by extrapolation) a late-stage domain growth law of $l(t)\sim t^{1/3}$. In response, Mazenko and Valls[6(c)] have recently stated that their previous claim of a logarithmic growth law seems to be incorrect.

The CHC equation has also been the subject of considerable numerical work. It was solved by Petschek and Metiu[7(a)] and (without noise) by Miyazaki *et al.*[7(b)] However, they did not study the scaling regime. Recently, Gawlinski *et al.*[7(c)] reported a two-dimensional (2D) simulation of the CHC equation, and claim that $\phi\sim 0.33$ for all time.

With the aid of our deterministic CDS model,[15,14] Chakrabarti and Gunton[8] unambiguously confirmed the asymptotic growth exponent $\frac{1}{3}$ (for about two decades *without* extrapolation). Thus we can conclude that the growth exponent for the conserved-order-parameter case is $\frac{1}{3}$ and that our CDS scheme gives this. This exponent is the one theoretically predicted by Kawasaki and Ohta.[12(a),12(c)] Thus in this paper, although the time dependence of the length scale will be exhibited, our main concern is the form factor. In the Appendix we give our derivation of interface equations and exponents.

III. CELL DYNAMICAL SYSTEM MODELS

Given the numerical effort involved in simulating the CHC equation or performing a Monte Carlo simulation, it is desirable to have computationally efficient models to study the scaling regime. Recent developments suggest that CDS models may fill such a need.[8]

A cell dynamical system is a space-time discrete dynamical system with a variable defined on each lattice point, which is updated in discrete time steps. The state of the lattice at a given time step is usually a function of the state at previous time steps. Cellular automata[16(a)] (CA) and coupled maps[16(b),16(c)] are examples of CDS's. The CDS approach has been successfully used for some time; notable examples are those in Refs. 16–18.

A. Deterministic models (summary of part I)

In part I, we explained our motivation for our intuitive construction of CDS models for phase-ordering dynamics. We presented deterministic CDS models for both the nonconserved- and conserved-order-parameter cases. The essential idea underlying our modeling is that the temporal evolution of the order parameter $\psi(t,n)$ associated with a lattice site labeled by n at time t is governed by the following two mechanisms.

(a) The local driving force (which is due to the chemical potential).

(b) The diffusive effect due to the difference of the order-parameter values in the neighboring cells.

The first mechanism dictates the tendency of an individual cell in the absence of connecting cells or other constraints (e.g., conservation of the order parameter). Below the critical temperature, we expect the order parameter of an individual cell to approach either of two nonzero values $\pm\psi_0$ (corresponding to the two symmetric minima of the ϕ^4 free energy below the critical temperature), depending on the initial value $\psi(0,n)$. We model this tendency on a coarse-grained time scale by an injection f on $\mathbf{R}$ (the set of real numbers) with two symmetric (about the origin) hyperbolic sinks and one hyperbolic source at the origin (corresponding to the unique high-temperature minimum of the ϕ^4 free-energy functional). Thus the single-cell dyamics is described by

$$\psi(t+1,n)=f(\psi(t,n)) \ . \tag{3.1}$$

We choose $f(x)$ to be $A\tanh x$ throughout this paper.

We model the second mechanism by incorporating into the update a diffusive contribution (in the absence of the constraint that order parameter be conserved) proportional to the difference of the order parameter in a cell from the average order parameter in the neighboring cells. Thus our deterministic model for the nonconserved case reads

$$\begin{aligned}\psi(t+1,n)&=f(\psi(t,n))+D[\langle\langle\psi(t,n)\rangle\rangle-\psi(t,n)]\\&\equiv\mathcal{T}[\psi(t,n)] \ ,\end{aligned} \tag{3.2}$$

where D is a positive constant proportional to the phenomenological diffusion constant, and $\langle\langle * \rangle\rangle - *$ is essentially the isotropized discrete Laplacian. We use the following definition of $\langle\langle * \rangle\rangle$ on the two-dimensional square lattice:

$$\langle\langle\psi(t,n)\rangle\rangle=\tfrac{1}{6}\sum(\psi \text{ in the nearest-neighbor cells})+\tfrac{1}{12}\sum(\psi \text{ in the next-nearest-neighbor cells}) \ . \tag{3.3}$$

The isotropic choice of the local averaging in (3.3) is crucial in the conserved-order-parameter case so as not to introduce an unphysical anisotropy into our results, as we demonstrated in part I.

For the conserved case, we must respect the restriction that order parameter cannot be created or destroyed in exchanges between neighboring cells. Thus, in an exchange of order parameter between a cell and its neighboring cells, there should not be a net change of order parameter inside the neighborhood of the central cell. Since the net gain of the order parameter by the center cell is given by $\mathcal{T}[\psi(t,n)]-\psi(t,n)$, the simplest (deterministic) discrete model for the conserved case reads

$$\psi(t+1,n)=\mathcal{T}[\psi(t,n)]-\langle\langle\mathcal{T}[\psi(t,n)]-\psi(t,n)\rangle\rangle \ . \tag{3.4}$$

In (3.4) the subtraction corresponds to the extra Laplacian in the CHC equation.

Thus we have arrived at deterministic CDS models. The models are intrinsically computationally efficient and ideally suited to a parallel computation environment. However, we did not use array processors for any of the demonstrations in part I or in this paper. We were able (due to computational efficiency) to get sufficiently long-time behavior using a VAX-750 computer as we demonstrate in this paper.

In part I, we used these models and demonstrated the potential of our scheme. The salient points made in part I were as follows.

(i) Asymptotic results are unchanged even if we change the map f *as long as* we respect the conditions that it be injective and that it have two hyperbolic sinks symmetrically placed about one hyperbolic source. We call this the "structural stability" of our modeling.

(ii) We proposed a class of new discretization schemes for semilinear parabolic PDE's which relate CDS models and corresponding PDE models. We emphasize, however, that we do not require PDE's to arrive at CDS models. By definition, any numerical simulation of a PDE is a simulation of a CDS, so that by default no numerical simulation of PDE's can be faster or more efficient than CDS simulations.

B. Addition of stochasticity to models of part I

It is generally believed that the noise effect is unimportant for late stages of phase-separation kinetics.[19] As far as we are aware, the issue has not yet been settled analytically or numerically and is of considerable interest. For the conserved order parameter case, we addressed this problem numerically in a recent letter[20] and our results indicate that the effects of noise are asymptotically irrelevant. In this paper, we expand on these results. Specifically, we compare the form factors for both the nonconserved and conserved cases without and with noise.

We can put noise into our model for the nonconserved case by analogy with the TDGL equation (2.1),

$$\psi(t+1,n)=\mathcal{T}[\psi(t,n)]+B\eta(t,n) \ , \tag{3.5}$$

where B (the noise amplitude) is a third parameter in our model (the others being D and the parameter A in f). The noise $\eta(t,n)$ is a random number (uniformly distributed in $[-1,1]$) assigned at each time t to each lattice site $n[\equiv(n_x,n_y)]$. We have also performed simulations in which noise has a Gaussian distribution and this made no difference to our results.

If we regard our CDS models as arising from a discretization (albeit an unconventional one) of the corresponding PDE as described in part I, the noise amplitude B is related to the kinetic coefficient and the discretization mesh size through the fluctuation-dissipation theorem. Thus, changing B would correspond to changing the ki-

netic coefficient, if we keep the mesh size fixed. However, as in the usual deterministic TDGL equation, we simply discard the noise while retaining the nonzero kinetic coefficient, ignoring the fluctuation-dissipation theorem. Thus our comparison in Secs. IV and V will be between the deterministic case (which does not satisfy the fluctuation-dissipation theorem) and the noisy case (which satisfies the fluctuation-dissipation theorem). It should be noted, furthermore, that irrespective of the parameters of the quenched thermodynamic potential we expect the asymptotic behaviors to be universal. This is borne out by our results in part I.

To add noise to our model for the conserved case, we proceed in analogy with the CHC equation. In (2.1), we can use for the noise

$$\sigma(\mathbf{r},t)=\nabla\cdot\boldsymbol{\eta}(\mathbf{r},t)\ , \tag{3.6}$$

where $\boldsymbol{\eta}(\mathbf{r},t)$ is a vector white noise with Gaussian components which satisfy the usual fluctuation-dissipation relation

$$\langle \eta_i(\mathbf{r},t)\eta_j(\mathbf{r}',t')\rangle = 2L\delta_{ij}\delta(\mathbf{r}-\mathbf{r}')\delta(t-t')\ . \tag{3.7}$$

It is easily verified that $\sigma(\mathbf{r},t)$ as defined by (3.6) satisfies the conditions (2.3). Thus, in our discrete space-time model, we include noise as

$$\begin{aligned}\psi(t+1,n)=\mathcal{F}[\psi(t,n)]-\langle\langle\mathcal{F}[\psi(t,n)]-\psi(t,n)\rangle\rangle \\ +B[\eta_x(t,n_x+1,n_y)-\eta_x(t,n_x,n_y) \\ +\eta_y(t,n_x,n_y+1)-\eta_y(t,n_x,n_y)]\ ,\end{aligned} \tag{3.8}$$

where B is again a third parameter in the model. The noise vector $(\eta_x\eta_y)(t,n)$ consists of two random numbers distributed as in the nonconserved case. The one-sided discretization used for the form $\nabla\cdot\boldsymbol{\eta}(\mathbf{r},t)$ in (3.8) is not crucial. We have confirmed that our results are not affected if we use a center-difference scheme to discretize $\nabla\cdot\boldsymbol{\eta}(\mathbf{r},t)$.

Our results in Ref. 20 and in Secs. IV and V support the theoretical view that the effect of noise is irrelevant for asymptotic results.

C. Correspondence to reality and to other numerical simulations

Strictly speaking, there is no fundamentally reliable way of choosing parameters (including "real" values of the lattice spacing and time step) in our models other than comparing the results (for different parameter values) from our models (e.g., the time evolution of patterns) with experimental results. As will be clear from the demonstrations in Sec. IV and V, a study of the asymptotic regime does not (because of extensive universality) determine a unique set of parameters. To determine the parameters in our model which correspond to a particular experimental situation, we have to look at the nonuniversal behaviors. If we specify a functional form of the map in our model beforehand, we can estimate necessary parameters by analyzing experimental results for nonuniversal quantities such as the interface thickness, the wave vector of the unstable mode in the early stages (viz., the Cahn-Hilliard regime), the rate of growth of this unstable mode, etc. However, it is not our goal to model nonuniversal features and so we do not try to determine here a set of parameters that may correspond to a particular situation. Notice that the statements made above are also valid for the conventional models such as the TDGL equation or the CHC equation.

Comparison of our results with those of other numerical simulations also faces the same problems as those outlined above. Therefore, here we confine ourselves only to making a few relevant comments on the real values of our lattice spacing and time steps in the case with conserved order parameter. Similar comparisons are possible for the nonconserved case also, but we do not present those here.

Our general goal is the simulation of coarse-grained dynamics as in the conventional PDE and models such as the CHC equation. Thus a single cell in our model definitely does not correspond to a single atom in an experiment or a single spin in a Monte Carlo simulation. A rough estimate of the size of our lattice spacing in the conserved case may be obtained in several ways as follows.

(a) We can compare our results for the crossover of the growth exponent in the case of the critical quench (described in Sec. VI) with the recent results of Gaulin *et al.*[3(b)] (we should warn the reader that this is only a very rough comparison because the experiment is in 3D, whereas our simulation is in 2D). They see a crossover in the exponent to its asymptotic value of $\phi\sim 0.33$ when the peak of the form factor is about 20 Å^{-1}. Therefore the length scale of the pattern is about 40π Å, which is the width of 30–40 atoms. In our deterministic simulation with $A=1.3$ and $D=0.5$, we see a crossover from $\phi\sim 0.28$ to the asymptotic value of $\phi\sim 0.33$ when the pattern size is about ten lattice spacings. If we assume that the exponent crossover occurs at the same representative pattern size in both cases, a single lattice spacing in our model would contain about 3–4 atoms. Thus, a single cell in our 2D model corresponds to about 3^2 (say, 10) atoms.

An estimate of the time step in our simulation may be obtained by comparing the crossover time in our simulation with that of Gaulin *et al.*[3(b)] They observe a crossover to the asymptotic exponent at about 4100 sec. In our simulation, the crossover is at about 2750 iterations. Thus our time step is about 1.5 sec in the Gaulin *et al.* experiment.

(b) We can also estimate the size of a single cell in our model in terms of a Monte Carlo simulation by looking at, say, the interfacial boundary structure. Since there are only two values allowed to each spin in a Monte Carlo simulation (of the Ising model), one may be tempted to say that the wall is always sharp. But this is not true because the walls in a Monte Carlo simulation are always ragged on the microscopic scale (see, e.g., Gawlinski *et al.*,[4] Huse[6(b)]). The true thickness of the wall is obtained after the raggedness has been averaged out. Thus the amplitude of the raggedness is a measure of the actual thickness of the wall. From the representative patterns of, e.g., Huse[6(b)] for the conserved case, it is clear that the

wall thickness is about 4–5 spins. In our deterministic simulation with $A=1.3$ and $D=0.5$, the wall thickness is about 1–2 lattice spacings. Hence a single cell in our model has a width of about 2–3 spins (at least). Hence, again a single cell in our 2D simulation contains about ten spins.

To estimate the time step in our simulation (in terms of Monte Carlo steps), we compare our results with those of Grest and Srolovitz[4] for the conserved case. Grest and Srolovitz obtain their results on a 400×400 lattice. They define a Monte Carlo step (MCS) as 400^2 spin-exchange attempts for the entire lattice, viz., an average of one spin-exchange attempt per spin. At 3×10^4 MCS, their representative pattern width is about ten spins. In our simulation, we reach a corresponding pattern width (viz., about three lattice spacings) at about 23 steps. Thus the time step in our model corresponds to about 1300 MCS. Again, if we assume that representative pattern sizes in our simulation and the Monte Carlo simulation are comparable when the exponent crossover from $\phi\sim0.25$ to ~0.33 takes place, the Monte Carlo simulation of Grest and Srolovitz would crossover into the asymptotic regime at a pattern width of about 30 spins. Therefore, $3\times10^4\times3^4$ $(=2.43\times10^6)$ MCS are necessary for a crossover to the asymptotic regime.

Finally, we deal with the objection that the model used in Monte Carlo simulations is far more realistic than the coarse-grained model used in CDS or conventional partial-differential-equation models. At first glance, this argument may appear convincing. But we do not believe there is any hard evidence to support this. On the contrary, as pointed out by Binder,[13(b)], it is doubtful whether Kawasaki exchange dynamics is realistic because of the difficulty of the two-particle exchange. This is because there is no local concerted movement of atoms which could speed up the exchange of the atoms. Furthermore, the Monte Carlo simulation does not account for the presence of vacancies or lattice defects. We believe that metastable freezing encountered in Monte Carlo simulations may be a result of their being somewhat unrealistic.

IV. RESULTS FOR CASE WITH NONCONSERVED ORDER PARAMETER

A. Deterministic case

All of our demonstrations for the nonconserved case are for a two-dimensional 150×150 lattice with periodic boundary conditions. All form factors are calculated as averages of 20 independent runs. This sample size is not sufficiently large to conclusively determine the form factor for small values of k, since there is no self-averaging near $k=0$, but is large enough to study the exponent and

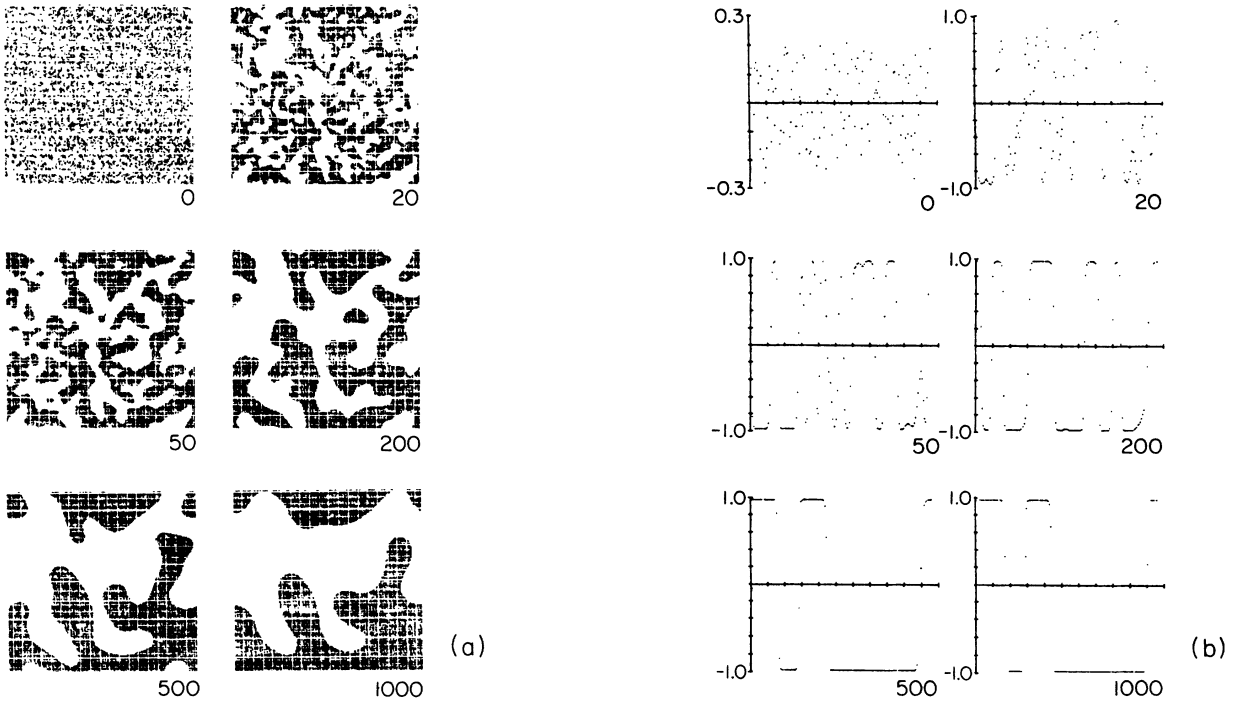

FIG. 1. (a) Evolution pattern for the nonconserved case (without noise) for a 150×150 lattice. The initial configuration (labeled by 0) has order-parameter values uniformly and randomly distributed between ±0.125. The numbers denote necessary time steps from the initial condition. Only points with positive order parameter are marked. This coding is also used in all subsequent evolution patterns we display in this paper. (b) Evolution of the domain-wall structure for the situation shown in (a). The figures correspond to the variation of the order parameter along the diagonal from $(n_x=1,n_y=1)$ to $(n_x=150,n_y=150)$; the segment between adjacent horizontal tick marks corresponds to about 14 diagonal lattice elements. The numbers along the vertical axes denote the order-parameter values. Again, the integers denote the number of time steps from the initial condition. Well-defined walls (about 1–2 sites thick) are formed by about 50 updates.

the large-k behavior of the form factor. The parameter values used in this section are always $A=1.3$ and $D=0.5$. These parameter values correspond to a deep quench. All calculations were done on a VAX-750 computer (without using any array processors). For the nonconserved case, a single update of the lattice took 3.60 CPU seconds. We have *not*, as yet, introduced a lookup table for the local dynamics.

Evolution patterns and domain-wall structures

Figure 1(a) shows a typical evolution pattern using (3.2) resulting from a random initial configuration, i.e., with order parameter values uniformly and randomly distributed between ± 0.125 (labeled by 0 in the figure). We use the same random initial condition for evolution patterns displayed throughout this section. As can be seen from Fig. 1(a), well-developed patterns appear within 20 updates. By about 500 updates, the pattern has coarsened to such an extent that we expect finite-size effects to be important. In Fig. 1(b), we show the change in domain-wall structures for the evolution shown in Fig. 1(a). The pictures correspond to the variation of the order parameter along the diagonal from $(n_x=1,n_y=1)$ to $(n_x=150,n_y=150)$. The times at which these sections are taken are the same as those for the patterns of Fig. 1(a). As can be seen from Fig. 1(b), well-defined walls (which are 1–2 sites thick) are formed by about 50 updates. Hence we may expect asymptotic behaviors beyond 50 times steps.

Behavior of $\langle k \rangle(t)$

We define $\langle k \rangle(t)$ as

$$\langle k \rangle(t)=\int_0^\infty dk\, kS(\mathbf{k},t)\Big/\int_0^\infty dk\, S(\mathbf{k},t)\ . \tag{4.1}$$

This is related to the typical domain size as $\langle k \rangle(t) \propto l(t)^{-1}$. Note that $\langle k \rangle(t)$ is *not* the true average with respect to $S(\mathbf{k},t)$,

$$\bar{k}(t)=\int_0^\infty dk\, k^d S(\mathbf{k},t)\Big/\int_0^\infty dk\, k^{d-1}S(\mathbf{k},t)\ . \tag{4.2}$$

In the case with infinitesimally thin walls, the quantity $\bar{k}(t)$ is divergent as a result of Porod's law,[27(b)] which predicts that the tail of the form factor decays as $k^{-(d+1)}$ in d dimensions.

Numerically, we compute $\langle k \rangle(t)$ by considering all $\mathbf{k}$ values up to half the reciprocal lattice size. Notice that $\mathbf{k}$ can take values (for a lattice of size $N\times N$) $2\pi(m_x,m_y)/N$, where m_x and m_y have integer values between $-N/2$ and $(N/2)-1$. We should point out that, in the deterministic cases of this section (and Sec. V), the tails of the form factors decay rapidly enough that the

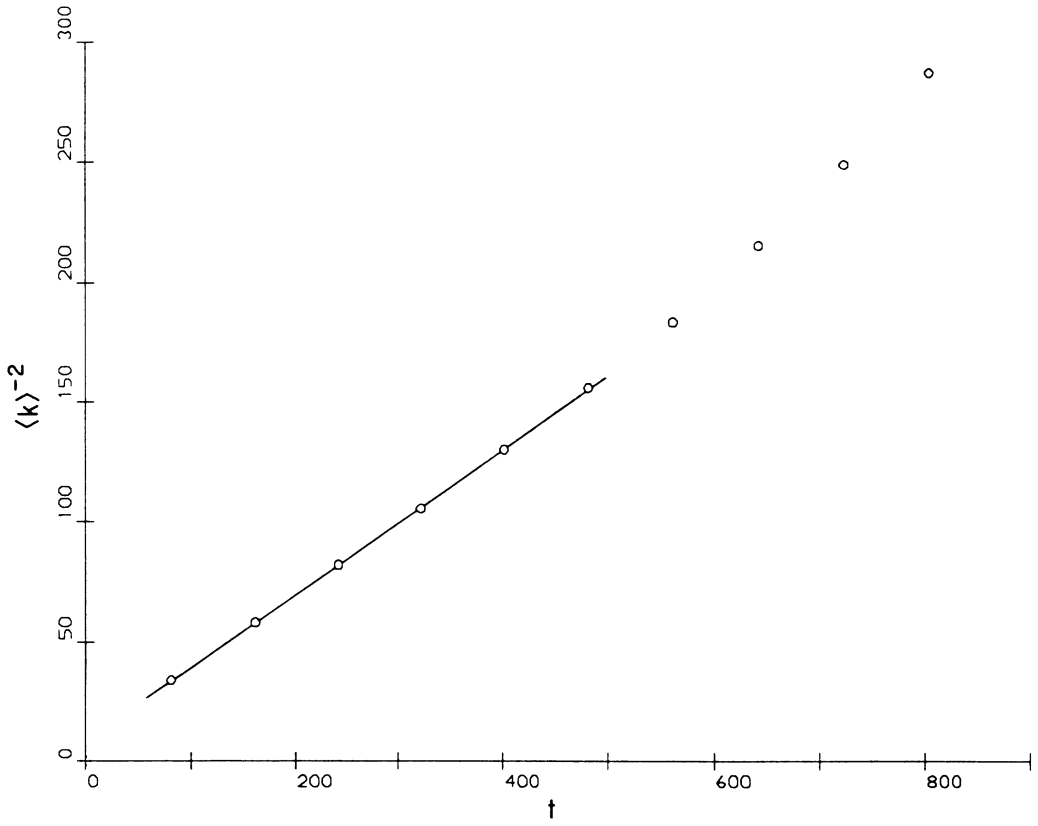

FIG. 2. Plot of $\langle k \rangle(t)^{-2}$ vs t for the nonconserved case (without noise) for a 150×150 lattice. The times are from 80 to 800 in steps of 80. As is expected, up to ~ 500 data lie on a straight line, but beyond this finite-size effects make the effective exponent larger than $\frac{1}{2}$.

value of $\langle k \rangle(t)$ is almost unchanged even if we include the entire reciprocal lattice in our calculation. (In the noisy case of this section, viz., the nonconserved case with noise, the value of $\langle k \rangle(t)$ is again almost unchanged if we include the entire reciprocal lattice.) In the conserved case with noise, the value of $\langle k \rangle(t)$ is slightly changed if we include a larger fraction of the reciprocal lattice size, but the exponents (and their crossovers) *remain unchanged.* From the various experiments and numerical simulations already described, we expect the characteristic domain size to behave as $(t-t_0)^{1/2}$ between 50 and ~ 500 updates. This is demonstrated in Fig. 2. Beyond this time domain the completion of the ordering process is speeded up because the average curvature increases due to the finite-size effect. This was confirmed by our simulations on smaller lattice sizes, which showed a transition to an exponent greater than $\frac{1}{2}$ at earlier times than the 150×150 lattice.

Scaling of form factors

We should point out that, in what follows, we always demonstrate scaling in the form [different from (2.4)]

$$S(\mathbf{k},t)=[\langle k \rangle(t)]^{-d}\Phi(k/\langle k \rangle(t)) , \tag{4.3}$$

where d is the dimensionality. This should be satisfied as long as there exists a unique characteristic length scale in the evolution process.

In Fig. 3(a), we have plotted $S(k,t)\langle k \rangle(t)^2$ as a function of $k/\langle k \rangle(t)$ for times 160, 480, and 800. For small values of k, $S(k,t)$ does not have the self-averaging property, so that we cannot get a reliable functional form near the origin. However, this does not affect appreciably the normalization of the form factor and the calculation of $\langle k \rangle$. The raw data of the form factor are defined as a function of vector $\mathbf{k}$ rather than scalar k. To scalarize our data, we average it over shells of inner radius $(n-1)\delta k$ [with $\delta k=(2\pi/N)\times 0.5$, N being the lattice size] and outer radius $n\delta k$ (where n is an integer) in the Brillouin zone. The scalar function thus obtained is what we term $S(k,t)$ and the corresponding k value is assigned as $(n-1)\delta k+\delta k/2$ (except in the case $n=0$, where the corresponding k value is assigned as 0). The first few $S(k,t)$ values represent averages over very few $\mathbf{k}$ values. For example, $S(0,t)$ has a contribution only from the $\mathbf{k}=2\pi(0,0)/N$ value. Thus the statistics for the small-k values is not good. However, as is demonstrated in Sec. IV B, our numerical results combined with an analytical discussion can provide a strong support for the OJK functional form[11(c)] for the form factor.

Porod's law and Tomita's sum rule

Tomita[21(a)] studied the real-space form factor $S(\mathbf{r},t)$ for the late stages of phase-ordering dynamics. From very general considerations (applicable to both the nonconserved and conserved cases), he derived a small-r form of $S(\mathbf{r},t)$ from which he derived Porod's law,[2(b)]

$$S(\mathbf{k},t)=\int d\mathbf{r}\, e^{i\mathbf{k}\cdot\mathbf{r}}S(\mathbf{r},t) \sim \frac{A(t)}{k^{d+1}} \quad \text{for } k\to\infty , \tag{4.4}$$

where $A(t)$ is positive. He also derived the following sum rule (known as Tomita's sum rule):

$$\int_0^\infty dk\,[k^{d+1}S(\mathbf{k},t)-A(t)]=0 . \tag{4.5}$$

It should be noted that in the present context large k implies that $kl(t)$ is large. Hence the absolute value of k can be very small. Here we show that even a very small finite thickness of the domain walls results in a gross violation of Porod's law and Tomita's sum rule.[21(c)]

Consider the interface between two regions which are rich in the opposing phases [respectively labeled by $\psi(\mathbf{r},t)=\pm\psi_0$]. The position of the interface is labeled by $\mathbf{r}_i(\mathbf{a},t)$, where $\mathbf{a}$ is a $(d-1)$-dimensional vector which parametrizes the interface. The position of the interface is defined through $\psi(\mathbf{r}_i(\mathbf{a},t),t)=0$. Let n be the local coordinate which is perpendicular to the interface in its tubular neighborhood. Then we can locally write

$$\nabla\psi(\mathbf{r},t)=\frac{\partial\psi(n,t)}{\partial n}\hat{\mathbf{n}}(\mathbf{r},t) , \tag{4.6}$$

where $\hat{\mathbf{n}}(\mathbf{r},t)$ is the unit vector locally normal to the interface which points in the direction of $\mathbf{r}$. If we assume that the structure of the interface is translationally invariant along the interface (this is compatible with a subsequent assumption), we have

$$\nabla^2\psi(\mathbf{r},t)=\frac{\partial^2\psi(n,t)}{\partial n^2}+\frac{\partial\psi(n,t)}{\partial n}\nabla\cdot\hat{\mathbf{n}}(\mathbf{r},t) . \tag{4.7}$$

Let us introduce a field $u(\mathbf{r},t)$ through

$$\psi(\mathbf{r},t)=\psi_0\eta(u(\mathbf{r},t)/\delta) , \tag{4.8}$$

where $\eta(x)$ is a smooth, invertible function such that $\eta(0)=0$ and $\eta(x/\delta)$ weakly converges to $\mathrm{sgn}(x)$ in the $\delta\to 0$ limit. The position of the interface also satisfies $u(\mathbf{r}_i(\mathbf{a},t),t)=0$. Following Allen and Cahn,[2(b)] we assume that the interface has only a small curvature and that the domain wall locally (along the normal) has an equilibrium, static profile. Hence the TDGL equation (in the tubular neighborhood of the interface) has the form

$$\frac{\partial\psi(n,t)}{\partial t}=L\frac{\partial\psi(n,t)}{\partial n}\nabla\cdot\hat{\mathbf{n}}(\mathbf{r},t) \tag{4.9}$$

or (returning to Cartesian coordinates)

$$\frac{\partial\psi(\mathbf{r},t)}{\partial t}=L[\nabla\psi(\mathbf{r},t)\cdot\hat{\mathbf{n}}(\mathbf{r},t)]\nabla\cdot\hat{\mathbf{n}}(\mathbf{r},t) , \tag{4.10}$$

where the unit normal vector $\hat{\mathbf{n}}(\mathbf{r},t)$ is given by

$$\hat{\mathbf{n}}(\mathbf{r},t)=\left.\frac{\nabla' u(\mathbf{r}',t)}{|\nabla' u(\mathbf{r}',t)|}\right|_{\mathbf{r}'=\mathbf{r}_i} , \tag{4.11}$$

where $\mathbf{r}_i$ is the point on the interface which lies on the normal (to the interface) through $\mathbf{r}$. Clearly, for points $\mathbf{r}$ on the interface, we have $\mathbf{r}_i(\mathbf{a}_p,t)=\mathbf{r}$. Using the nonlinear transformation (4.8), we can write (4.10) as an equation (still nonlinear) for $u(\mathbf{r},t)$,

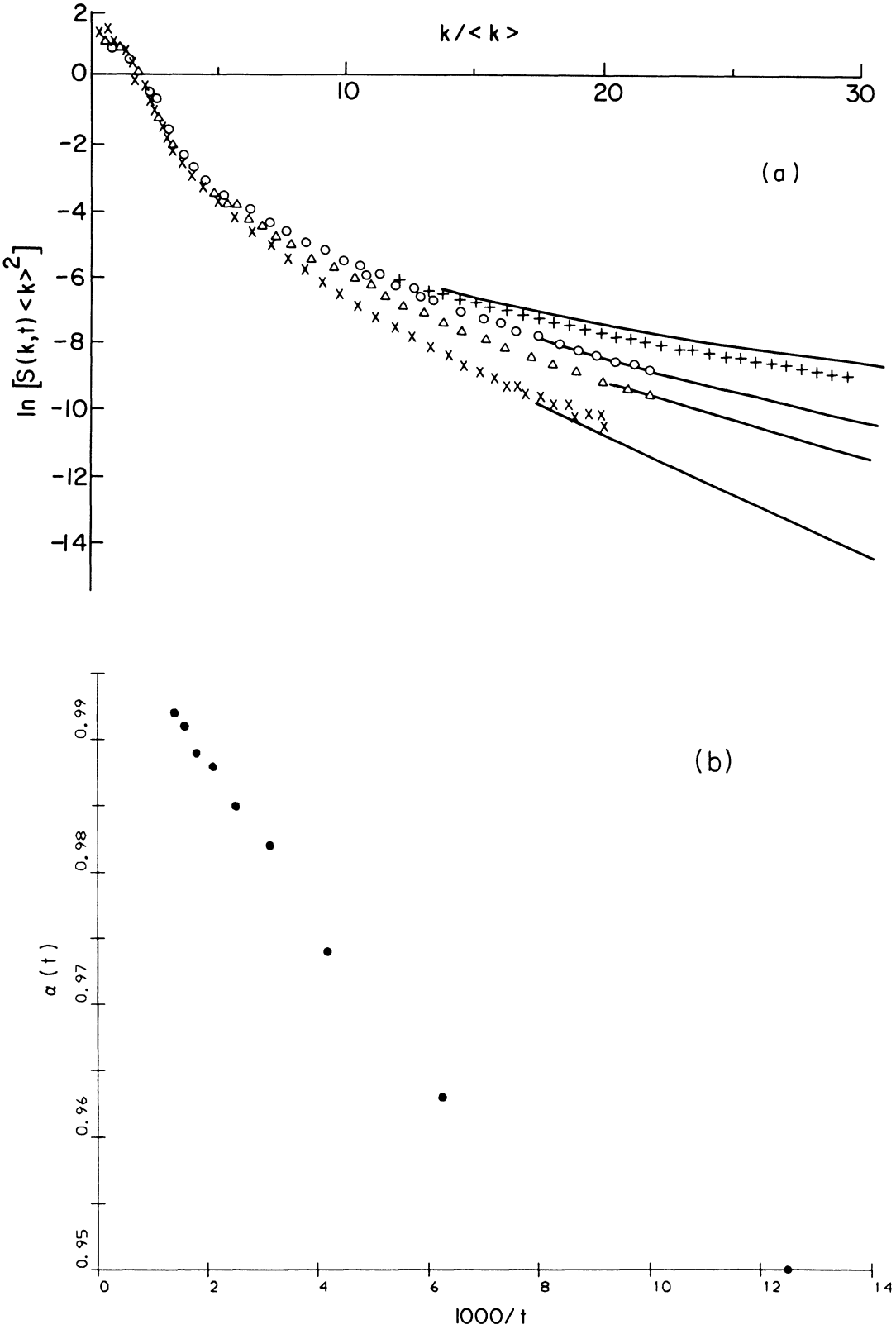

FIG. 3. (a) Scaled form factors for the nonconserved case (without noise) for a 150×150 lattice. Data from times 160, 480, and 800 are denoted, respectively, by $\times$, Δ, and $\circ$. The solid lines denote the results of (4.16). For each time step $\alpha(t)$ is adjusted as follows: for $t=160$ ($\times$), $\alpha=0.963$; for $t=480$ ($\triangle$), $\alpha=0.988$; and for $t=800$ ($\circ$), $\alpha=0.994$. The top curve is for $\alpha=1$, i.e., the OJK result, and the $+$ for $\alpha=0.999$. (b) α necessary to fit the numerical results [as explained in (a)] as a function of time. The figure demonstrates (4.17).

$$\frac{\psi_0}{\delta}\eta'(x)\left|_{x=\frac{u(\mathbf{r},t)}{\delta}}\right.\frac{\partial u(\mathbf{r},t)}{\partial t}=L\frac{\psi_0}{\delta}\eta'(x)\left|_{x=\frac{u(\mathbf{r},t)}{\delta}}\right.\nabla u(\mathbf{r},t)\cdot\left[\frac{\nabla' u(\mathbf{r}',t)}{|\nabla' u(\mathbf{r}',t)|}\left|_{\mathbf{r}'=\mathbf{r}_i(\mathbf{a}_p,t)}\right.\right]\cdot\left[\nabla\cdot\left[\frac{\nabla' u(\mathbf{r}',t)}{|\nabla' u(\mathbf{r}',t)|}\left|_{\mathbf{r}'=\mathbf{r}_i(\mathbf{a}_p,t)}\right.\right]\right]. \tag{4.12}$$

In (4.12), the term

$$\frac{1}{\delta}\eta'(x)\left|_{x=\frac{u(\mathbf{r},t)}{\delta}}\right.$$

is sharply peaked about $u(\mathbf{r},t)=0$ in the $\delta\to 0$ limit (when it weakly converges to the δ function). Furthermore, $u(\mathbf{r},t)$ is a rather slowly varying function, even in the tubular neighborhood of the interface. Thus we can drop the $\mathbf{r}'=\mathbf{r}_i(\mathbf{a}_p,t)$ condition in the definition of $\hat{\mathbf{n}}(\mathbf{r},t)$. This yields (near the interface)

$$\frac{\partial u(\mathbf{r},t)}{\partial t}=L\left[\nabla^2 u(\mathbf{r},t)-\sum_{\alpha,\beta}\hat{n}_\alpha(\mathbf{r},t)\hat{n}_\beta(\mathbf{r},t)\nabla_\alpha\nabla_\beta u(\mathbf{r},t)\right]+h(u(\mathbf{r},t),t)\ , \tag{4.13}$$

where $\hat{n}_\alpha(\mathbf{r},t)$ is the projection of $\hat{\mathbf{n}}(\mathbf{r},t)$ along the x_α axis, $\nabla_\alpha\equiv\partial/\partial x_\alpha$, and $h(u,t)$ is a function of $u(\mathbf{r},t)$ and t which weakly converges (in the $\delta\to 0$ limit) to a tempered distribution satisfying $h(u,t)\delta(u)=0$. The term $h(u,t)$ can only be neglected asymptotically (as we see later). The function $h(u,t)$ must be odd in u since (4.13) must be invariant under the transformation $u\to -u$. We assume that u is maximally smooth, so that $h(u,t)$ is analytic in u. Then, near the interface (where u is small) we may assume that $h(u,t)=g(t)u$, where $g(t)$ is determined by the requirement that the wall thickness be invariant in time. (After all, the wall thickness should be independent of time in the asymptotic regime.)

Following Ohta *et al.*,[11(b)] we linerize (4.13) by replac-

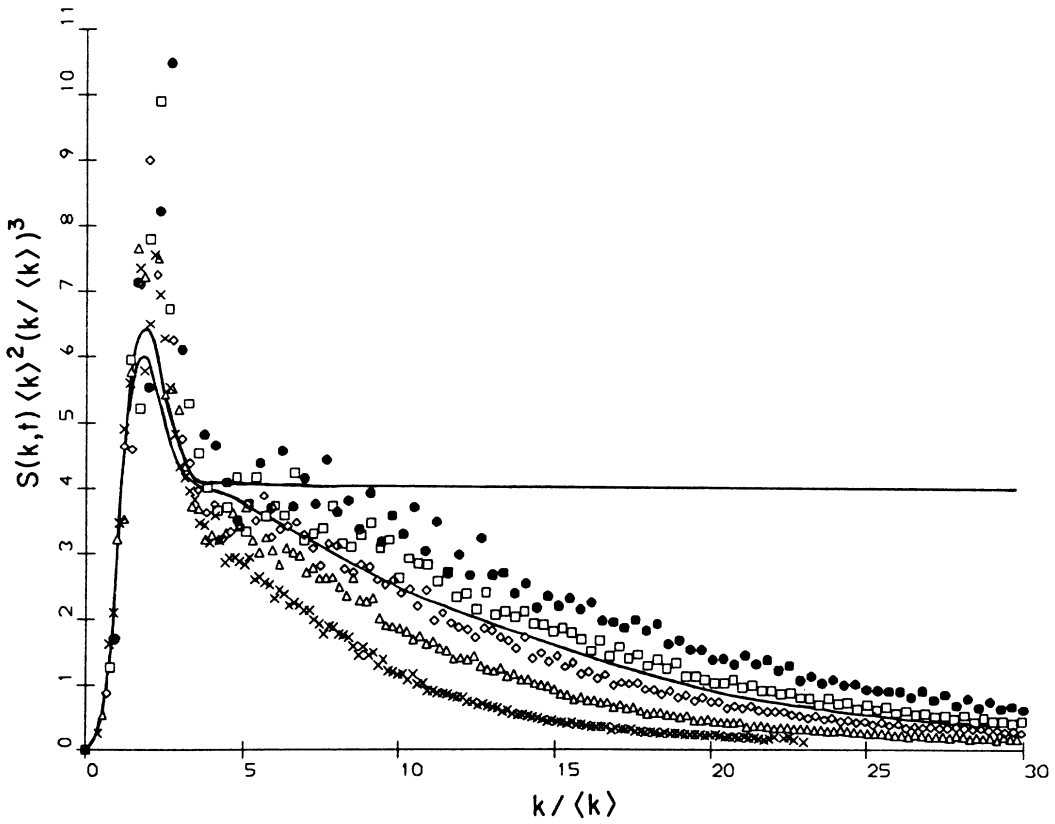

FIG. 4. Test of Porod's law (and Tomita's sum rule) for time 160 (×), 320 (△), 480 (◇), 640 (□), and 800 (●). The upper curve is the result of the OJK theory, and the lower curve is due to (4.16) with $\alpha=0.97$. The tail of our data decays faster than the Porod tail as a result of the finite thickness of the wall, and neither Porod's law nor Tomita's sum rule is satisfied, but the hump in the data is clearly the precursor of Porod's law. If we extend it to the left, Tomita's sum rule is also satisfied.

ing $\hat{n}_\alpha(\mathbf{r},t)\hat{n}_\beta(\mathbf{r},t)$ by the corresponding average over an ensemble of initial conditions, viz., $\langle \hat{n}_\alpha(\mathbf{r},t)\hat{n}_\beta(\mathbf{r},t)\rangle$. For an isotropic system,

$$\langle \hat{n}_\alpha(\mathbf{r},t)\hat{n}_\beta(\mathbf{r},t)\rangle = \frac{\delta_{\alpha\beta}}{d} , \tag{4.14}$$

where $\delta_{\alpha\beta}$ is the Kronecker δ. Thus (4.13) reduces to (near the interface)

$$\frac{\partial u(\mathbf{r},t)}{\partial t} = L\left[\frac{d-1}{d}\right]\nabla^2 u(\mathbf{r},t)+g(t)u(\mathbf{r},t) . \tag{4.15}$$

From the solution for $u(\mathbf{r},t)$ from (4.15), we see that $g(t)\sim(d+2)/4t^{-1}$ is required asymptotically to keep the wall thickness independent of time.

Assuming that the initial u field is Gaussian as in the OJK theory, and following exactly the OJK theory, we can calculate the correlation function from which we have obtained the scaled form factor in the deterministic nonconserved case with a finite domain-wall thickness,

$$\Phi(x,t)=\frac{1}{\sin^{-1}\alpha}\frac{(2\pi)^{d/2}}{x} \times\int_0^\infty dR\, R^d\frac{(xR)^{1-d/2}}{[\alpha(t)^{-2}e^{R^2}-1]}J_{d/2}(xR) , \tag{4.16}$$

where $\Phi(x,t)$ is defined analogously to $\Phi(x)$ in (2.4). In (4.16), $J_\nu(x)$ is the Bessel function of the first kind and

$$\alpha=\alpha(t)=(1+c/t)^{-1} , \tag{4.17}$$

with c being a numerical constant which we cannot calculate within the present theory. With $\alpha=1$ we recover the OJK analytic form.[11(b)] We can choose an appropriate c in (4.17) for all sufficiently long t as demonstrated in Fig. 3. Thus we may conclude that our CDS results asymptotically agree with the OJK theory result. From Fig. 4 we can actually recognize the precursor of the Porod's tail and Tomita's sum rule. The OJK result agrees with the result of Kawasaki *et al.*[11(a)] asymptotically. One may then be tempted to say that the present approach is equivalent to that of Kawasaki *et al.*[11(a)] This is not true. In the case of Kawasaki *et al.*,[11(a)] the ratio of the wall width and the pattern size goes to 0 exponentially fast, which is unphysical. In our present approach, the wall thickness is maintained constant, so that the ratio decays algebraically.

B. Effect of noise on the nonconserved case

Evolution patterns and domain-wall structures

Figure 5(a) shows the evolution pattern for the case with $A=1.3$, $D=0.5$ (as before), and $B=0.3$ (noisy case). A comparison with Fig. 1(a) shows that the domain boundaries for the noisy case are somewhat more ragged than in the noiseless case. In Fig. 5(b), we show the evolution of the domain-wall structures for the situation shown in Fig. 5(a). This time, the section is along the horizontal line in the middle. Here, the domains are not well formed and noise has the effect of introducing fluctuation even in the interior of a domain. (However,

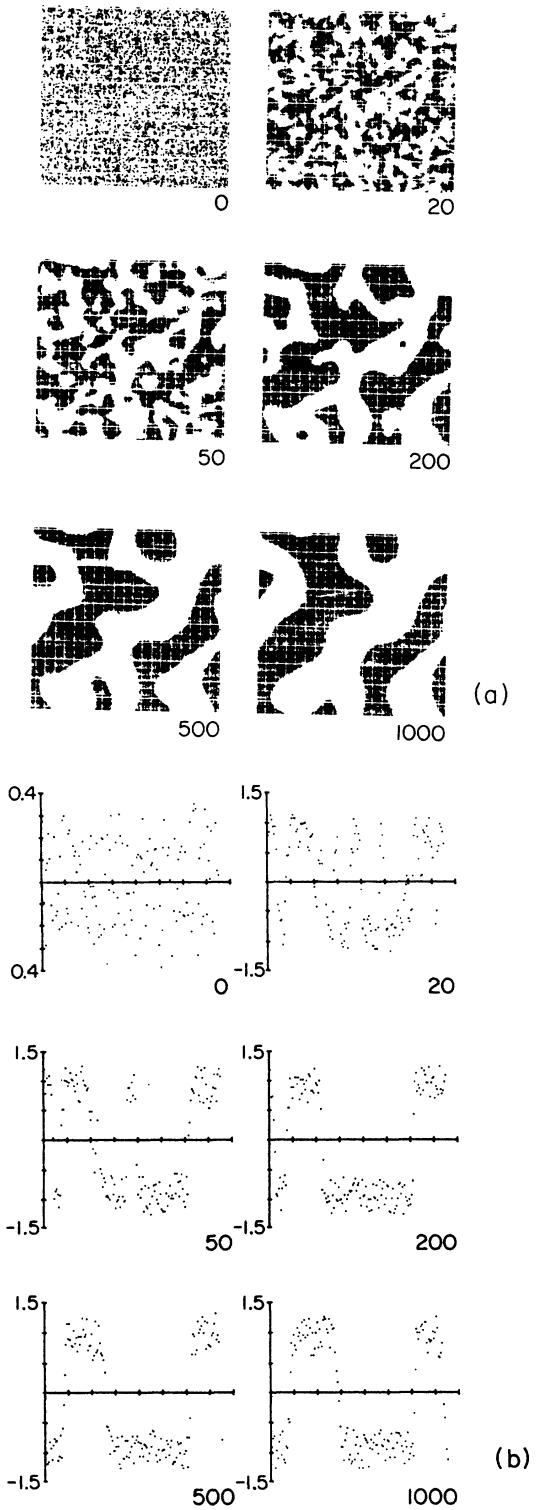

FIG. 5. (a) Evolution pattern for the nonconserved case with noise $B=0.3$ for a 150 lattice. The initial configuration is the same as in Fig. 1(a). The domain boundaries are somewhat more ragged than those of the deterministic case. (b) Evolution of the domain-wall structure for the situation shown in (a). However, this time the section is along the horizontal line in the middle. For numbers see the legend for Fig. 1(a). The segment between adjacent horizontal tick marks corresponds to about 14 lattices. The noise amplitude used is unrealistically large and the domains are not very well formed.

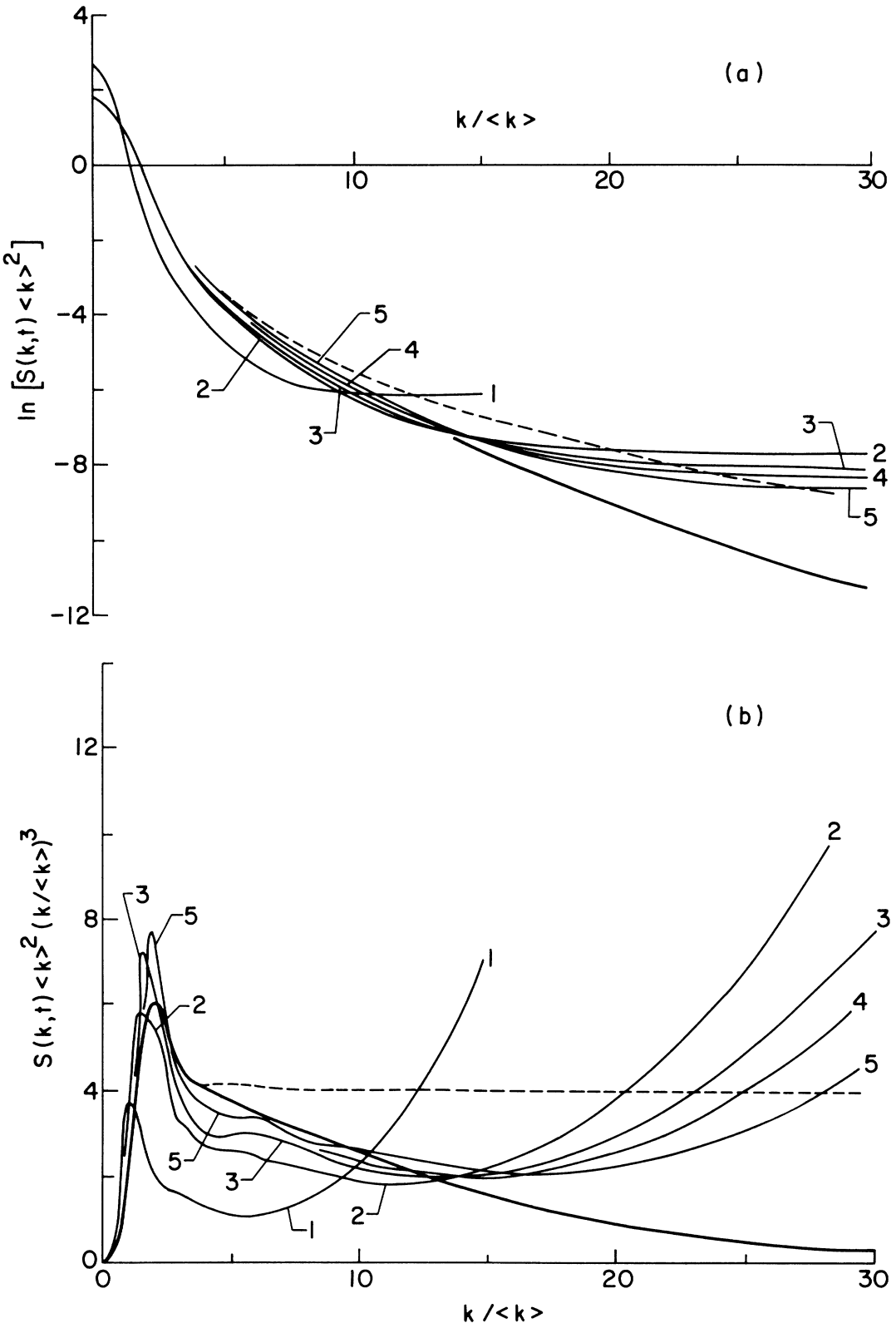

FIG. 6. (a) Semilogarithmic plot of the data corresponding to Fig. 5(a). In this case, the tails decay slower than the Porod tail and have the same qualitative behavior as in the Monte Carlo case due to the raggedness of the interface. The time steps are as follows: 1, $t=160$; 2, $t=320$; 3, $t=480$; 4, $t=640$; and 5, $t=800$. Although for small k the results for later times are not reliable due to the finite-size effect, for $k/\langle k \rangle$ larger than about 10 there is no problem. The thick line denotes (4.16) with $\alpha=0.97$, and the dashed line denotes the OJK theory [i.e., (4.16) with $\alpha=1$]. (b) Test of Porod's law (and Tomita's sum rule) for the data corresponding to Fig. 5(a). The numbers and notations are the same as those in (a). The upward trend of data in the tail is the result of noise-induced raggedness at small length scales.

notice that $B=0.3$ is an unrealistically large noise.)

To demonstrate that the raggedness of the domain boundaries [seen in Fig. 5(a)] is not the result of a cumulative effect of the noise, we have performed a simulation in which we start with a noiseless evolution and then turn on the noise (with amplitude $B=0.3$) after 195 updates. Within a few updates, the domain boundaries become ragged again. Alternatively, we can demonstrate that the presence of noise is crucial to maintain the raggedness. Within a few updates after turning off the noise, the domain boundaries rapidly become smooth.

Scaling of form factors

In Figs. 6(a) and 6(b), we compare the scaled form factors for the noisy case (at times 160, 320, 480, 640, and 800) with the analytic form of Ohta *et al.*[11(b)] and the form (4.16) with $\alpha=0.97$. As before, the tails of the curves do not satisfy Porod's law[21(b)] (or Tomita's sum rule[21(a)]) and decay slower than x^{-3}, where $x=k/\langle k\rangle(t)$ (as in the Monte Carlo case). This is borne out by Fig. 6(b), where we have plotted $S(k,t)\langle k\rangle(t)^2\times[k/\langle k\rangle(t)]^3$ versus $k/\langle k\rangle(t)$. The upward trend of the curves for large values of $k/\langle k\rangle(t)$ is a consequence of noise-induced raggedness at very short length scales. A similar effect is seen in the Monte Carlo results.[4] Asymptotically, we expect that both Porod's law and Tomita's sum rule will be satisfied, because the effect of noise are not cumulative and becomes less perceptible with increase in the representative pattern size.

V. RESULTS FOR CASE WITH CONSERVED ORDER PARAMETER

A. Critical quench, deterministic case

A single update of (3.4) for a 100×100 lattice with periodic boundary conditions took 1.77 CPU seconds. Throughout this section, the parameter values we use are $A=1.3$, $D=0.5$, unless otherwise mentioned. As in the nonconserved case, we use 20 independent runs to calculate all form factors shown in this section. We can get sufficiently accurate form factors with this number of samples; an independent check of results in this section with more than 30 samples has been done by Yeung.[22] The case of critical quenching is the most interesting one and is analytically the least tractable. In our discrete case, this corresponds to $\sum_n \psi(t,n)=0$.

Evolution patterns and domain-wall structures

In Fig. 7(a) we show a typical evolution pattern resulting from (3.4) for long times. The initial condition used

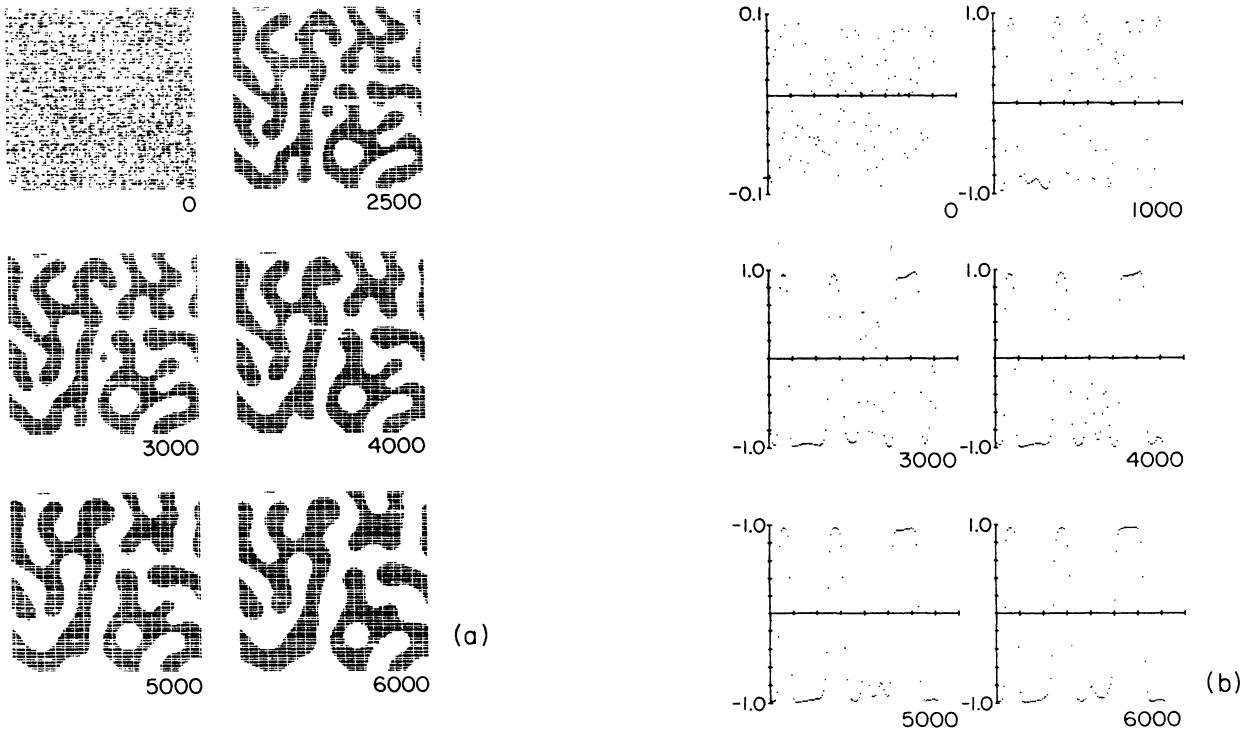

FIG. 7. (a) Evolution pattern for the conserved case (without noise) with a critical quench for a 100×100 lattice. The integers denote necessary updates. The initial configuration consists of order-parameter values randomly and uniformly distributed between ±0.125 as in Fig. 1(a). Of course, this corresponds to a different initial condition because of the different sizes of the lattices. (b) Evolution of the domain-wall structure for the situation shown in (a). The numbers along the vertical axes denote the order-parameter values, and the interval between the adjacent tick marks corresponds to about 13 lattice spacings. The times are the same as those in (a) except for the figure in the upper-right corner. It is taken at 1000 updates and indicates that well-formed domains appear by that time. The section is along the diagonal form $(n_x=1,n_y=1)$ to $(n_x=100,n_y=100)$, as in Fig. 5(a).

(labeled by 0) is one where the order parameter is uniformly and randomly distributed between ± 0.125. We use the same initial condition for all the evolution patterns in this section, unless specifically mentioned otherwise. In Fig. 7(b), we show the change in the domain-wall structures for the evolution shown in Fig. 7(a). The pictures correspond to the variation of the order parameter along the diagonal from $(n_x=1, n_y=1)$ to $(n_x=100, n_y=100)$. The time at which these sections are taken are the same as the times for the patterns of Fig. 7(a) except for the picture in the upper-right corner. It is taken at 1000 steps and shows that well-formed domains appear by about 1000 steps. The domains are fairly well defined and the wall thickness is about 2–3 sites.

Behavior of $\langle k \rangle(t)$ and growth exponents

We plot [in Fig. 8(a)] $\ln\langle k \rangle(t)$ versus $\ln t$ for this case for times 300–4500 in steps of 300. It is already known that the asymptotic exponent of our CDS model is $\frac{1}{3}$.[8] The curve shows that before reaching the asymptotic $\frac{1}{3}$ slope there is a regime with smaller exponent. The inset picture shows the data affinely transformed so as to clearly exhibit the crossover behavior.[22] There is a crossover at $t \sim 2750$ iterations from an exponent of $\phi \sim 0.28$ to the asymptotic value. The earlier time exponent $\phi \sim 0.28$ is compatible with a deterministic surface diffusion mechanism[10] which gives $\phi = \frac{1}{4}$, independent of the spatial dimensionality. A preliminary 3D simulation, however, does not exhibit this early regime, but only the asymptotic $\frac{1}{3}$ exponent.

In Fig. 8(b), we show a plot of $\langle k \rangle(t)^{-1}$ versus $t^{1/3}$ from early through late times. Up to about 80 iterations, a Cahn-Hilliard behavior is seen with $\langle k \rangle(t)^{-1}$ being more or less independent of time.[9] This crosses into a regime where $\phi \sim 0.28$ (deterministic surface diffusion regime), and this changes into the asymptotic regime with $\phi \sim 0.33$ at about 2750 iterations. This plot should be compared with Fig. 1 of the experimental results of Gaulin *et al.*,[3(b)] where a similar behavior is depicted.

Scaling of form factors

In Fig. 9(a) we have plotted $S(k,t)\langle k \rangle(t)^2$ as a function of $k/\langle k \rangle(t)$ for times 1800, 2400, 3000, 3600, and 4200. The data points can be seen to lie on a smooth master curve. The master nature of the curve is *insensitive* to the value of the growth exponent after ~ 2000 steps. Even for much earlier times we can achieve a reasonable master curve by this kind of superposition, as we have shown in Fig. 6 of part I. However, very long times cannot be fitted to this master curve.

Unfortunately, there is no theoretical prediction for us to make a comparison with. Our numerical curve does not satisfy Porod's law[21(b)] (or Tomita's sum rule[21(a)]). We do not even see a precursor to Porod's law. This is, however, consistent with the consequence of the finite thickness of the wall discussed in Sec. IV. Finally, for completeness, we plot [Fig. 9(b)] the real-space form factors. This is not for the demonstration of scaling, since the appearance of scaling is enhanced in this plot. This is because the small-k behavior is confined to the small amplitude tail of the real-space form factors. Recent papers from Gunton and co-workers[7(c),8] have plotted $S(r,t)$ versus $R_g(t)$, where $R_g(t)$ is the value of r at which $S(r,t)$ first goes to zero. We suspect that such plots see scaling considerably earlier than in our plots, as a result of the insensitivity of the real-space form factor.

B. Critical quench, noisy case

We have performed simulations using (3.8) with $B \leq 0.5$.

Evolution patterns and domain-wall structures

In Fig. 10(a) we show the patterns obtained for the noisy (with $B=0.3$) case. A comparison with Fig. 7(a) shows that the boundary walls are considerably more ragged than in the noiseless case (as in the nonconserved case). In Fig. 10(b), we show the change in the domain-wall structure. Again, as in the nonconserved case, the internal structure of the domains is made considerably ragged by the noise. (As we have pointed out before, the noise amplitude of $B=0.3$ is unrealistically high.)

To demonstrate that the raggedness is not the result of a cumulative effect of the noise, we studied the results of a simulation in which we started off with $B=0.0$ and then switched to $B=0.3$ after 3990 updates. The pattern quickly acquires ragged boundaries within ten updates. Alternatively, we studied the case where we turned off the noise (initially of amplitude $B=0.3$) after 3990 iterations. The boundaries become smooth within a few updates. Thus, as we have observed, it is highly unlikely that noise changes the asymptotic behaviors.

In Fig. 11, we show the evolution pattern for the strongly noisy (with $B=0.5$) case. This pattern is considerably more ragged than that for the case with $B=0.3$ and is similar to previously published patterns from Monte Carlo simulations[5,6(b)] or simulations of the CHC equation.[7]

Behavior of $\langle k \rangle(t)$ and growth exponents

In Fig. 12, we show $\ln\langle k \rangle(t)$ versus $\ln t$ for the noisy ($B=0.3$) case for times 2000–6200 in steps of 300. As in the deterministic case, the inset shows the data affinely transformed so as to accentuate the crossover. Here, the crossover to the asymptopia is delayed to $t \sim 3700$ iterations. Initially the exponent is $\phi \sim 0.27$. The general trend is that the crossover is delayed to later times for larger amplitudes of noise. We believe that this is because the ragged boundary of the pattern in the noisy case is equivalent (after coarse graining) to a "soft"

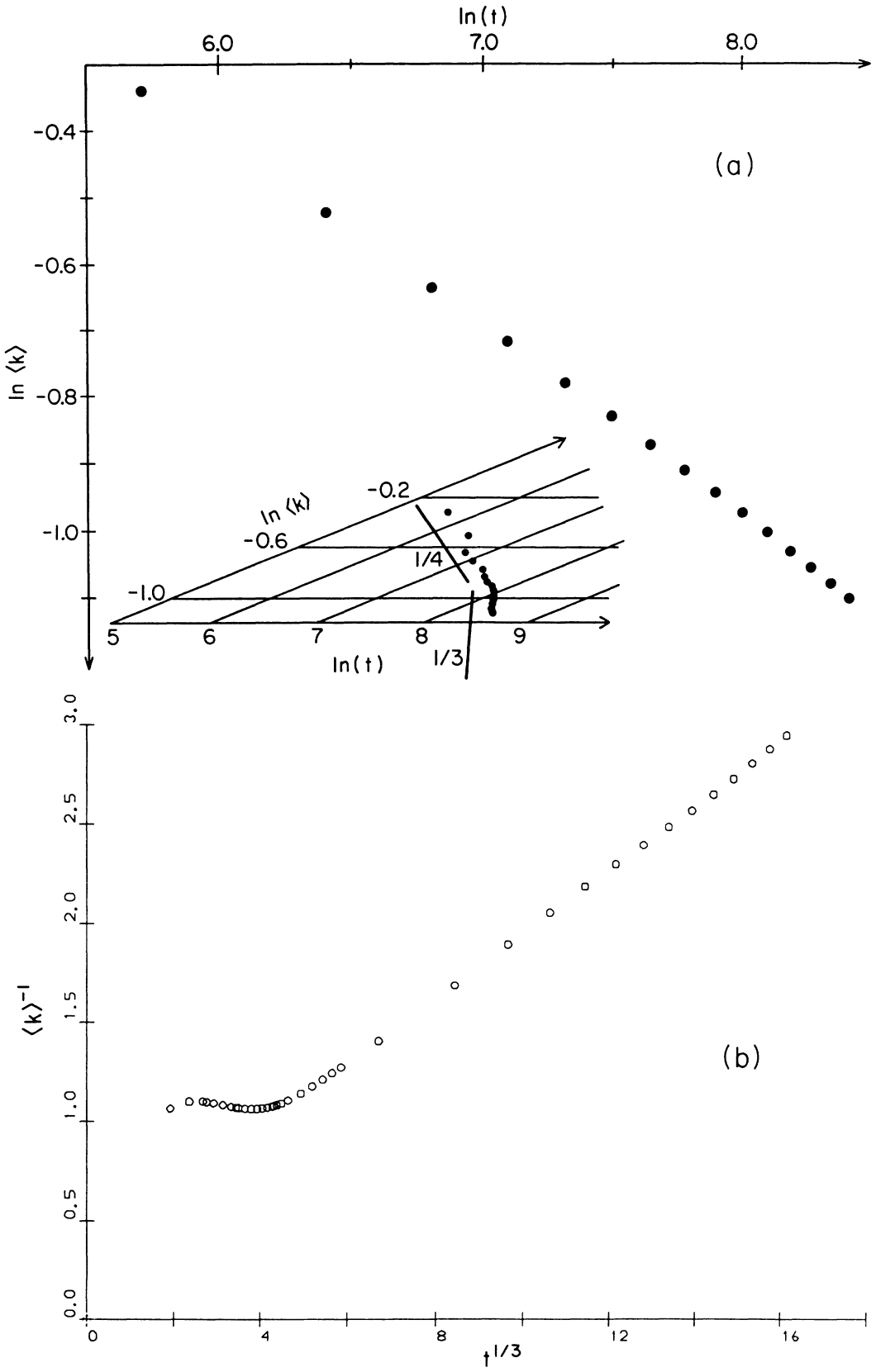

FIG. 8. (a) Plot of $\ln\langle k\rangle(t)$ vs $\ln t$ for the conserved case (without noise) with a critical quench for a 100×100 lattice. The times shown are from 300 to 4500 in steps of 300. The inset data shows the data affinely transformed so as to clearly exhibit the crossover behavior (Ref. 20) at about 2750 iterations. (b) Plot of $\langle k\rangle(t)^{-1}$ vs $t^{1/3}$ for early through late times (i.e., from 6 to 4500 iterations) for the critically quenched conserved case (without noise). The early times exhibits the linearized Cahn-Hilliard behavior.

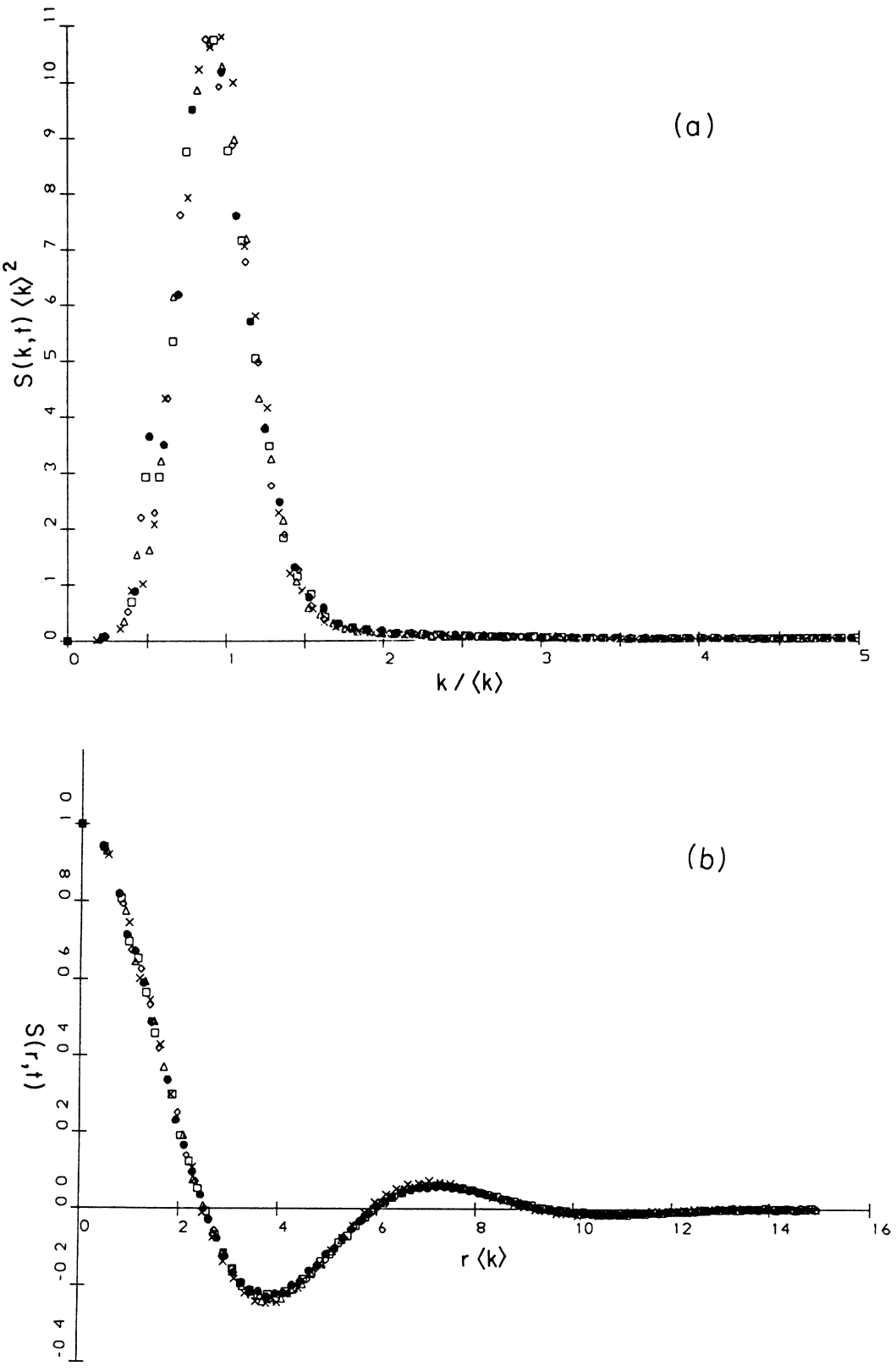

FIG. 9. (a) Scaled form factors for the consecutive case (without noise) with a critical quench for a 100×100 lattice. Data from times 1800 ($\times$), 2400 ($\triangle$), 3000 ($\Diamond$), 3600 ($\square$), and 4200 ($\bullet$) are superposed. These times correspond to both sides of an exponent crossover shown in Fig. 8(a). The master curve is different for earlier times, being sharper and with a larger amplitude (compare this figure with Fig. 6 of part I). (b) Real-space form factors for the data in (a). The symbols are the same as in (a).

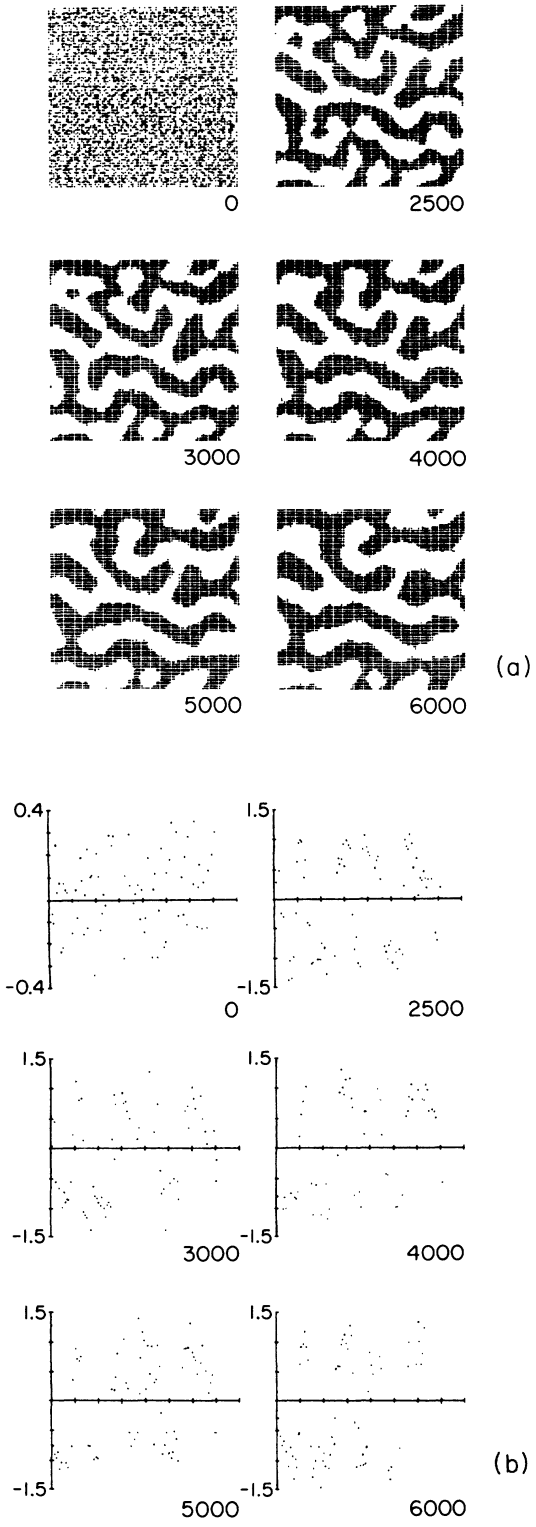

FIG. 10. (a) Evolution pattern for the conserved case (with noise $B=0.3$) with a critical quench for a 100×100 lattice. The integers denote necessary updates. The initial configuration is the same as in Fig. 7(a). (b) Evolution of the domain-wall structure for the situation shown in (a). For the numbers and tick marks in the figure see the legend for Fig. 7(b). The section is the same as in Fig. 7(b). As pointed out in the text, the noise amplitude used is unrealistically large and the domains are not well formed.

boundary wall. As we see in Sec. V C, the "soft-wall' evolution results in a delay of the exponent crossover. This is because the presence of soft walls enables the surface diffusion mechanism which has an associated exponent of $\phi=\frac{1}{4}$ in any dimension.

Scaling of form factors

In Fig. 13, we have superposed $S(\mathbf{k},t)\langle k\rangle(t)^2$ as a function of $k/\langle k\rangle(t)$ for times 2000, 2900, 3800, 4700, and 5600 for the noisy (with $B=0.3$) case. As in the deterministic case, the master curve does not depend sensitively on the value of the exponent for these late times. The resultant master curve is indistinguishable from the deterministic results [Fig. 9(a)]. For earlier times (500–2000), there is a different master curve with a higher peak which we do not show here. It is similar to the early-time master curve obtained for the deterministic case.

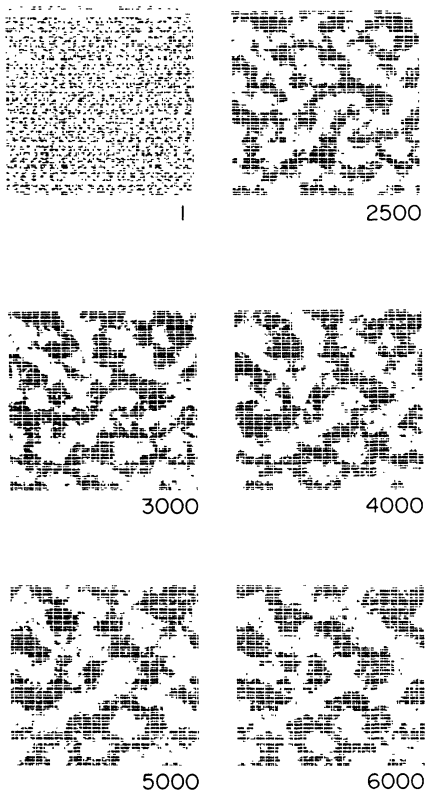

FIG. 11. Evolution pattern for the critically quenched conserved case with "strong" noise $B=0.5$ for a 100×100 lattice. The integers denote necessary updates. Once again, the initial configuration is the same as in Fig. 7(a). The pattern is similar to previously published patterns from Monte Carlo simulations [Refs. 5 and 6(b)] or Langevin simulations of the CHC equation (Ref. 7).

C. Critical quench, deterministic "soft-wall" case

As mentioned earlier, our parameter values correspond to a deep quench. This quickly results in sharp domain walls, whose thickness is negligible in comparison to the representative pattern size. This is the so-called "hard-wall" case. We can also simulate the so-called "soft-wall" case by considering a quench which is not so deep, i.e., by choosing A closer to 1. In this case, the domain wall thickness stays appreciable compared to the representative pattern size for a considerably longer time.

Evolution patterns and domain-wall structures

In Fig. 14(a), we show a representative evolution pattern for the deterministic soft-wall case, obtained by using $A=1.2$ and $D=0.5$ in (3.4). The corresponding change in the domain-wall structure is shown in Fig. 14(b). Comparing the domain-wall thickness in Figs. 7(b) and 14(b), one sees that the walls are somewhat thicker in Fig. 14(b). The effect is not strongly marked, though. The crossover occurs at about 4000 steps from $\phi \sim 0.27$ to ~ 0.33. The earlier exponent is compatible with a surface diffusion mechanism.

Scaling of form factors

In Fig. 15, we show the scaled form factors for the later times 4000, 4400, 4800, 5200, and 5600. This gives a master curve indistinguishable from the one we got for the deterministic case [Fig. 7(a)]. As expected, Porod's law does not hold and the decay of the tail is stronger than x^{-3}, where $x = k/\langle k \rangle(t)$.

VI. PRELIMINARY RESULTS FOR OFF-CRITICAL QUENCH

It is also possible to quench the system off-critically, i.e., $\int d\mathbf{r}\,\psi(\mathbf{r},t)$ has a nonzero value. Depending on whether the system is in an unstable state or a metastable state after quenching, the phase ordering proceeds via either spinodal decomposition or the so-called "nucleation process."

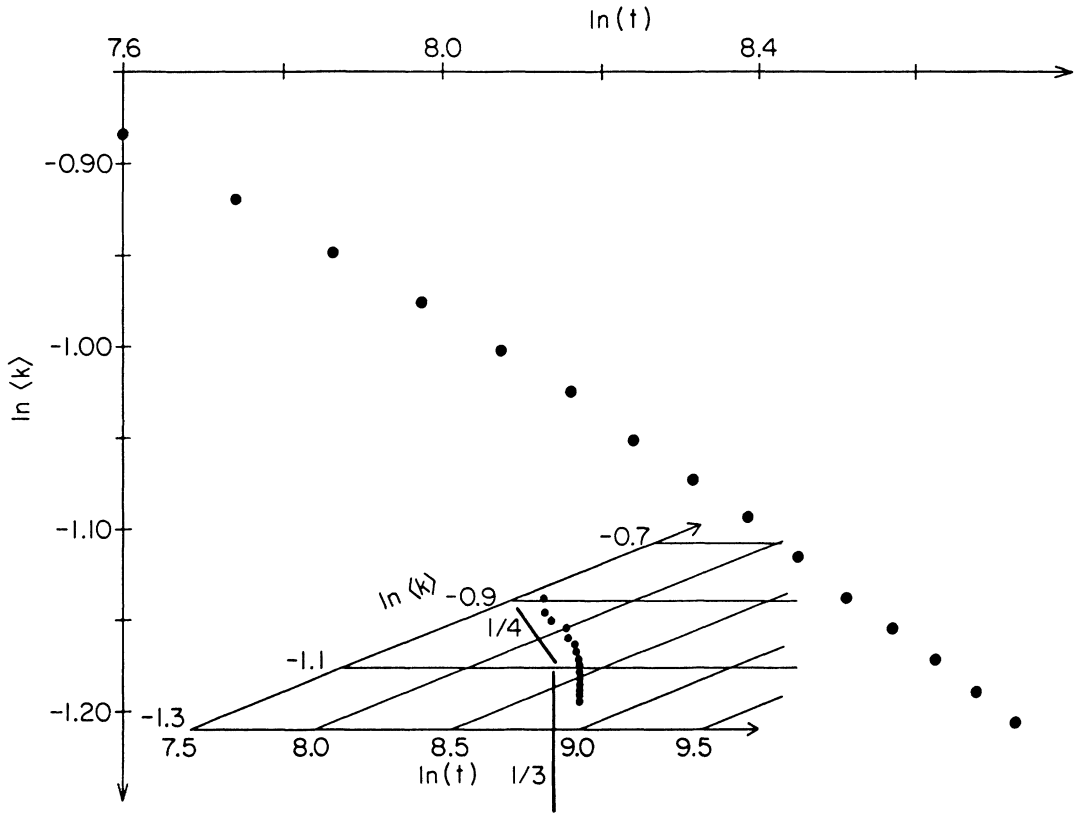

FIG. 12. Plot of $\ln\langle k \rangle(t)$ vs $\ln t$ for the critically quenched conserved case (with noise $B=0.3$) for a 100×100 lattice. The times are from 2000 to 6200 in steps of 300. As in Fig. 8(a), the inset picture shows the data affinely transformed so as to show the crossover in the exponent from $\phi \sim 0.27$ to ~ 0.33 more clearly. Here, the crossover is delayed to about 3700 iterations as a result of the softening of the walls by noise.

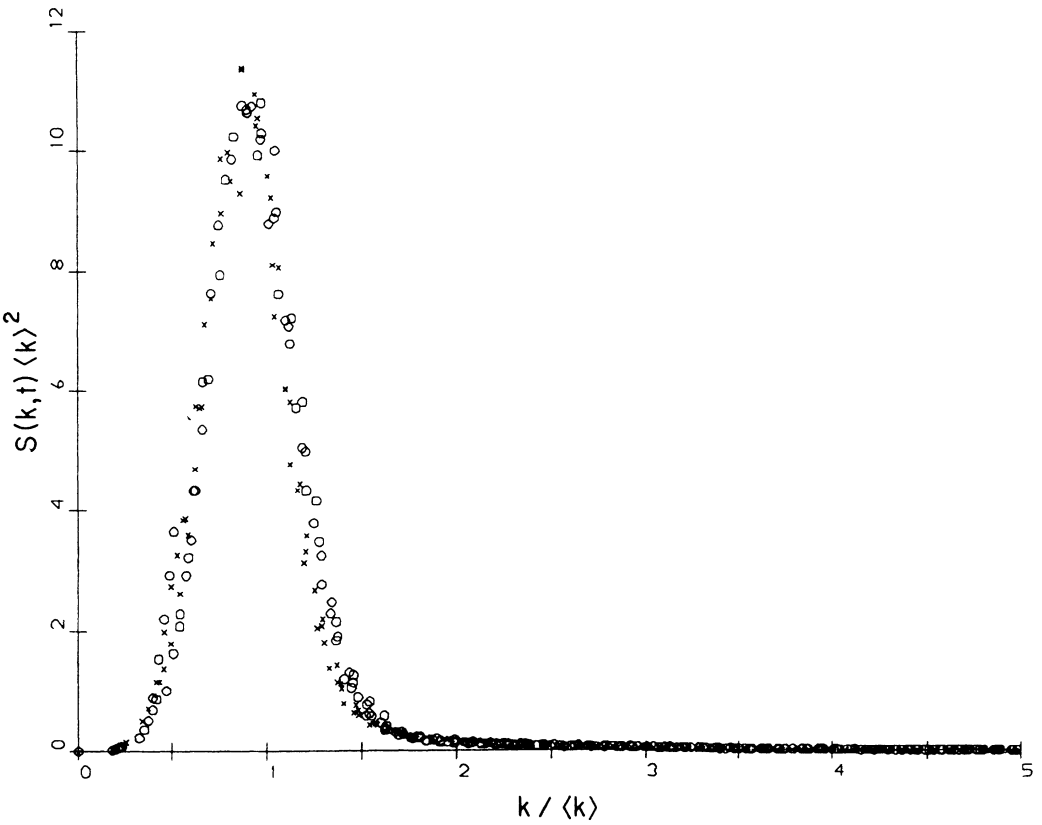

FIG. 13. Scaled form factors for the critically quenched conserved case (with noise $B=0.3$) for a 100×100 lattice are denoted by $\times$. Data from times 2000, 2900, 3800, 4700, and 5600 are superposed. $\circ$ denotes the scaled form factor without any noise given in Fig. 9(a). The master curve is indistinguishable from the one for the deterministic cases, demonstrating the irrelevance of noise.

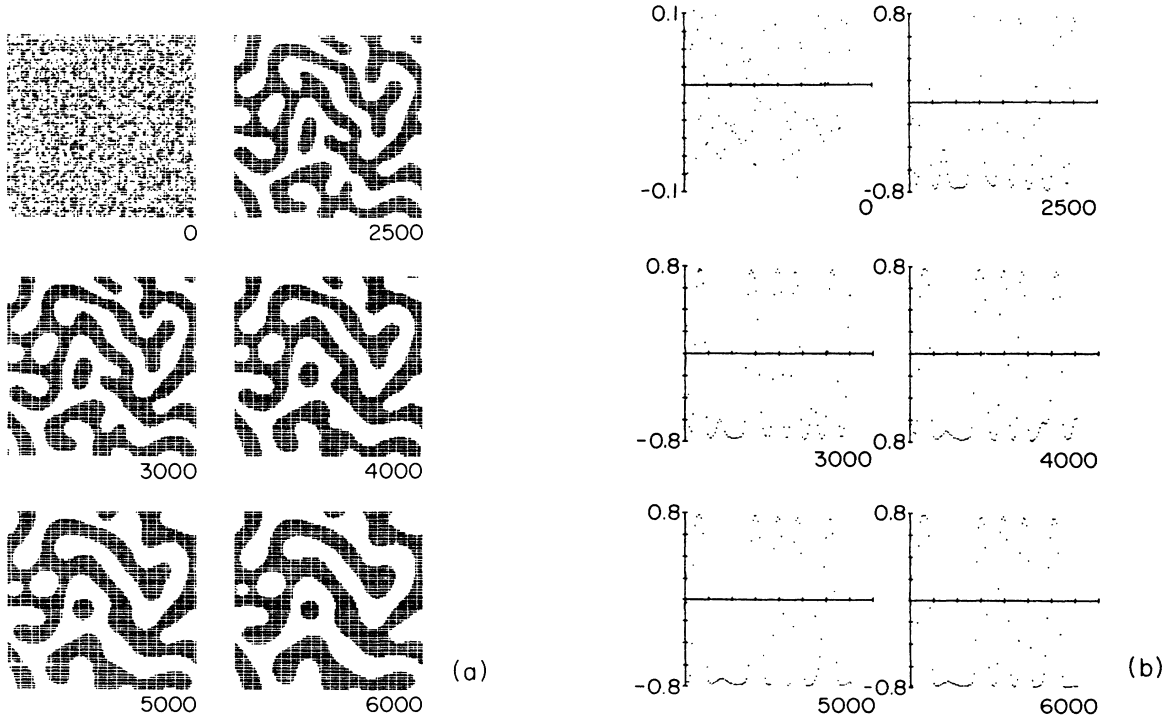

FIG. 14. (a) Evolution pattern for the "soft-wall" conserved case (without noise) with a critical quench for a 100×100 lattice. The integers denote necessary updates. The parameters used are $A=1.2$ and $D=0.5$. The initial configuration is the same as in Fig. 7(a). (b) Evolution of the domain-wall structure for the situation shown in (a). For the numbers and tick marks see the legend for Fig. 7(b). The section is the same as in Fig. 7(b). The domain walls are somewhat softer than those in Fig. 7(b).

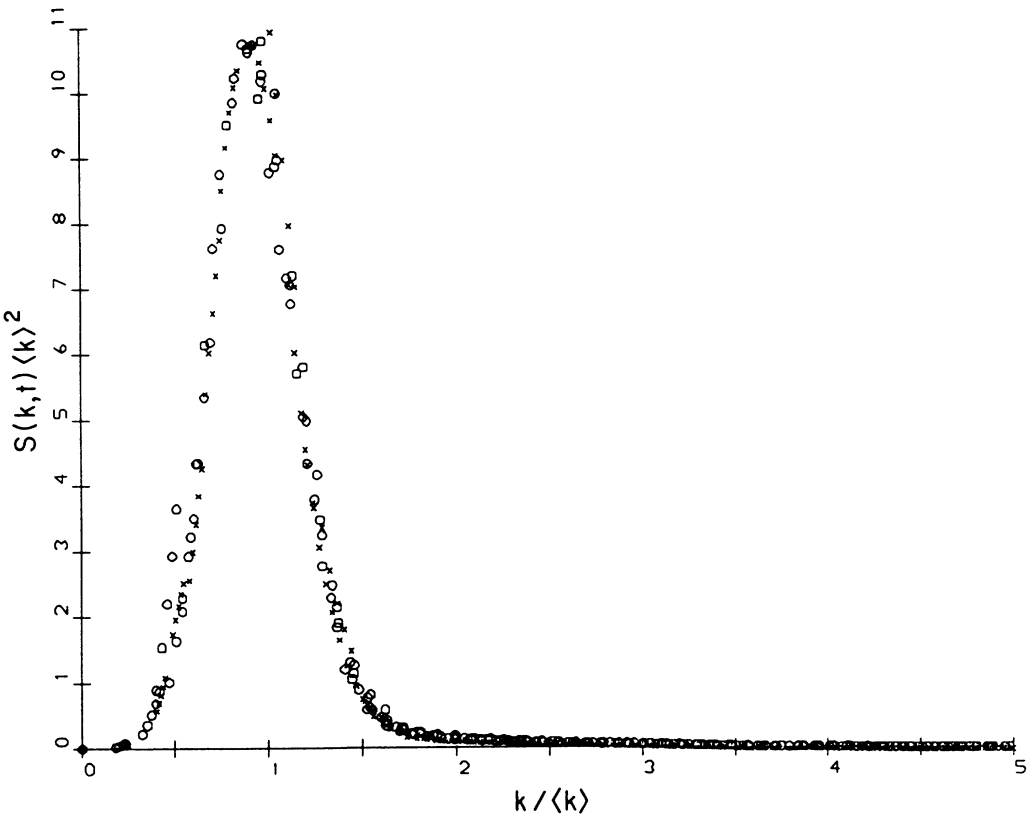

FIG. 15. Scaled form factors for the critically quenched "soft-wall" conserved case of Fig. 14(a) are denoted by $\times$. Data from later times 4000, 4400, 4800, 5200, and 5600 are superposed. $\circ$ denotes the form factor for the "hard-wall" case given in Fig. 9(a). The figure demonstrates the irrelevance of the quench depth to the asymptotic behavior.

In Fig. 16 we exhibit a noisy case ($B=0.3$) of off-critical spinodal decomposition. Brownian coagulation makes a well-developed pattern by 50 updates (which does not exist in the deterministic case). This mechanism corresponds to growth by the noise-induced diffusion and coalescence of small droplets of the minority phase. In Fig. 17, we plot the scaled form factors for this case from times 1200, 1600, 2000, 2400, and 2800. The exponent is still gradually increasing. The earlier exponent is compatible with the Brownian coagulation of humps on the domain boundaries. This mechanism has an associated exponent of $\phi=1/(d+3)$ in d dimensions, so that $\phi=0.20$ in 2D.

In a highly off-critical quench, the uniform state of the system is a metastable state. Segregation of phases can occur only if nucleation centers exist. In our deterministic model, we have to put in nucleation centers ("seeds") by hand. We simulate the nucleation regime by considering random initial configuration uniformly distributed between -0.6 ± 0.125 with randomly placed seeds (each consisting of at least four sites each and adding up to about 10% of the lattice) of order-parameter value $+0.98$. We then bias the sites with negative order parameter so that the average order parameter at each site is -0.6, corresponding to a minority species concentration of 20%. We study the noisy case by using (3.4) ($B=0.3$). Figure 18 shows the evolution pattern for this case. Here, it is evident that noise enables an evaporation-condensation mechanism and, in the later

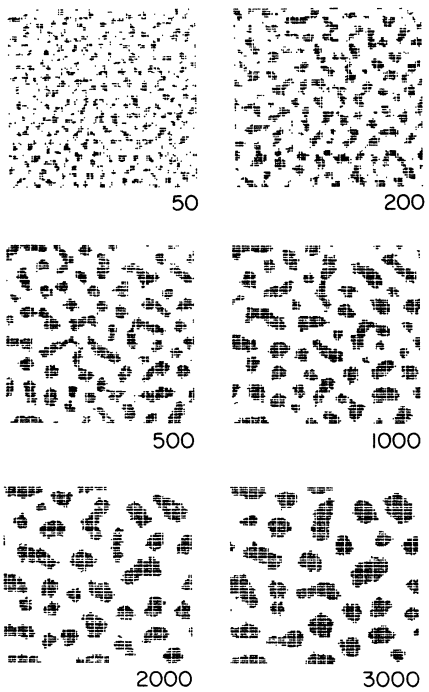

FIG. 16. Evolution pattern for the off-critically quenched conserved case (with noise $B=0.3$) for a 100×100 lattice. The initial configuration corresponds to the order parameter at the sites being randomly and uniformly distributed between -0.3 ± 0.125.

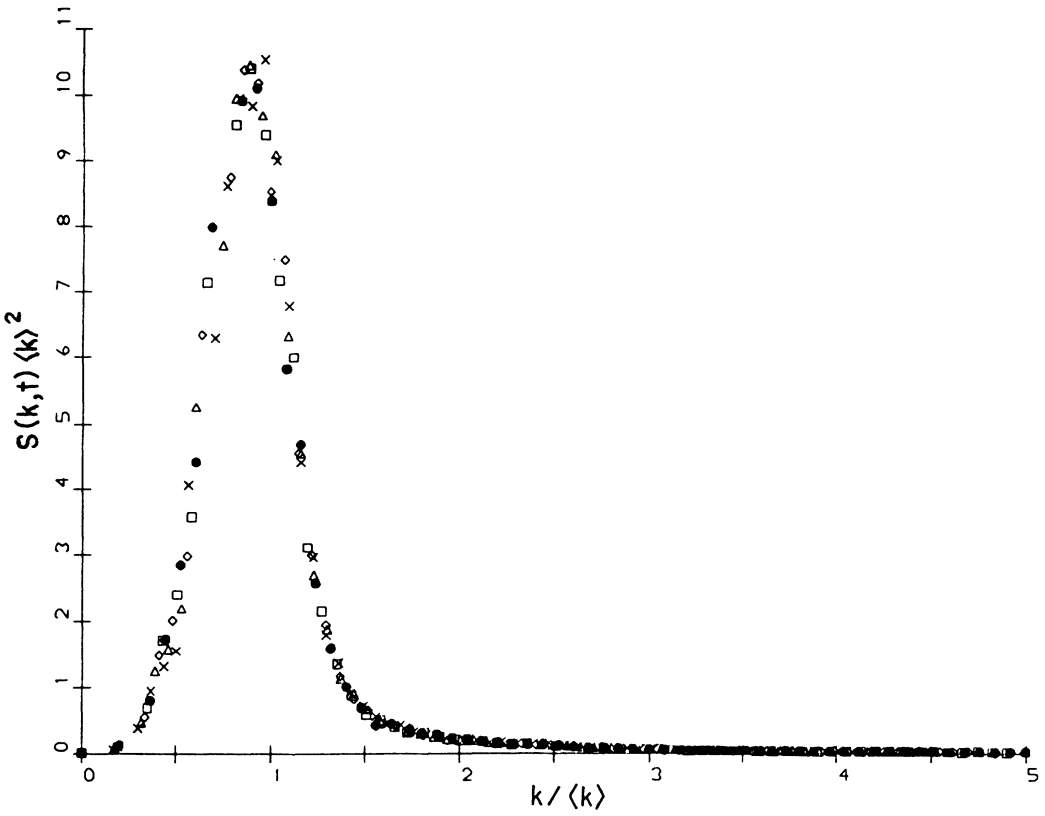

FIG. 17. Scaled form factors for the off-critically quenched conserved case of Fig. 16. Data from times 1200 (×), 1600 (△), 2000 (◇), 2400 (□), and 2800 (●) are superposed.

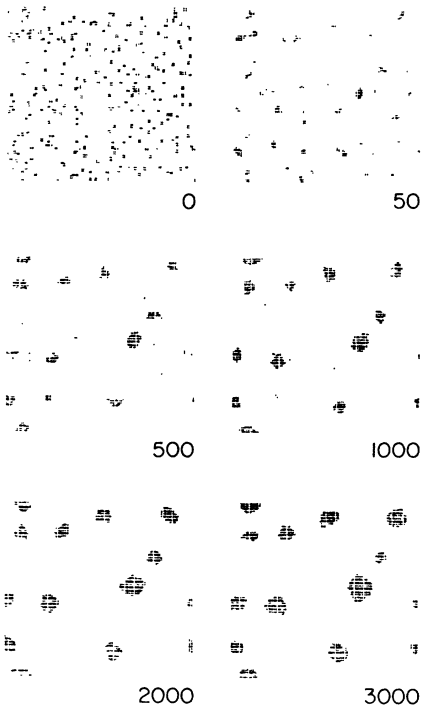

FIG. 18. Evolution pattern for the off-critically quenched conserved case (with noise $B=0.3$) with quenching in the nucleation regime. The integers denote necessary updates. Again, the lattice size is 100×100. For the initial configuration see the text.

stages, some droplets grow at the expense of others. The scaled form factors for this case (from times 1200, 1600, 2000, 2400, and 2800) are plotted in Fig. 19. The data points lie on a reasonable master curve. After the initial transition regime, the exponent is ~ 0.30.

VII. DISCUSSION AND SUMMARY

In part I of this exposition of the cell-dynamical-system modeling of phase-separation kinetics, we have (a) explained in detail how to construct CDS models, and (b) demonstrated the stability (or insensitivity) of our results to details of our models; and in this second part we have (c) exhibited the asymptotic form factors and their insensitivity to noise elements, and (d) presented preliminary results for the conserved case with an off-critical quench. We have also discussed in detail (in part I) a relation between the conventional PDE models and our CDS [or partial difference equation PΔE)] models. We emphasize that discretized stochastic PDE's with unjustifiably large time increments should be regarded as CDS's rather than as approximations to the continuum.

In this paper we have given a detailed study of the kinetics of phase ordering in 2D both without and with stochastic elements. We have provided evidence supporting the theoretical belief that stochastic elements are not important in the asymptotic regime. However, noise does have the effect of delaying the onset of the asymptotic regime. Larger noise amplitudes delay further the crossover from the earlier nonasymptotic regime to the later

asymptotic regime. Consequently, we expect it to be numerically very expensive to reach the asymptotic regime (if it is the same as that for the coarse-grained models) by means of Monte Carlo simulations. Of course, the Monte Carlo and Langevin models need not be in the same universality class.

Let us briefly summarize our results below.

Nonconserved case (1). The growth exponent ϕ is 0.5 but the finite-size effect is important at later times. The nonconserved dynamics is very rapid, so that the pattern rapidly covers an appreciable fraction of the lattice size. This leads to an increase in the average curvature, and an exponent larger than $\frac{1}{2}$ is seen for later times.

Nonconserved case (2). We have analytically explained the discrepancy between the form factor obtained by our CDS simulation and the theoretical result by Ohta, Jasnow, and Kawasaki. This comparison strongly suggests that the OJK result is accurate asymptotically, if not exact. Also this analytical study clarified the relation between numerical results and asymptotic laws such as Porod's rule and Tomita's sum rule.

Conserved case (1). The exponent ϕ for the conserved case exhibits a crossover from $\phi \sim 0.28$ to ~ 0.33. Our early-time exponent may be compatible with the exponent $\phi \sim 0.25$ seen by Mazenko and Valls[6(c)] in their Langevin simulation of the CHC equation. It can be explained by a deterministic surface diffusion mechanism (see Furukawa's review article in Ref. 1). Recently, Gawlinski *et al.*[7(c)] claimed to always see an exponent of 0.33 in their Langevin simulation of the CHC equation. This may be due to the differences between the quantities they used and those we used to analyze the raw data.

Conserved case (2). The master curve also shows a crossover from its earlier form to an asymptotic form. The crossover point seems to be always earlier than the crossover time for the exponent. (Notice, however, that an approximate master curve can be constructed well before the crossover time.) For the case with the critical quench, the early-time form is sharper than that for later times. (The opposite is true for the off-critical quench we study). We do not observe Porod's law (or Tomita's sum rule). This is not surprising because the evolution of the pattern is slow in the conserved case and the pattern size is not very large compared to the wall thickness.

Conserved case (3). For the critical quench, the quench depth affects only the crossover time; the asymptotic exponent and the master curve are insensitive to the quench depth (which determines wall thickness).

We believe that our models for the nonconserved case are in the same universality class as the TDGL equation, and those for the conserved case are in the same universality class as the CHC equation. This belief stems from our being able to derive our models by an appropriate discretization scheme, as described in part I. As we discussed briefly in the Appendix, we suspect that the Monte Carlo models of the conserved case (with Kawaskai exchange) are not precisely in the same universality class as the CHC equation, if they are quenched deeply. Rather, they may be in a different universality class along with what we have termed the Langer (or

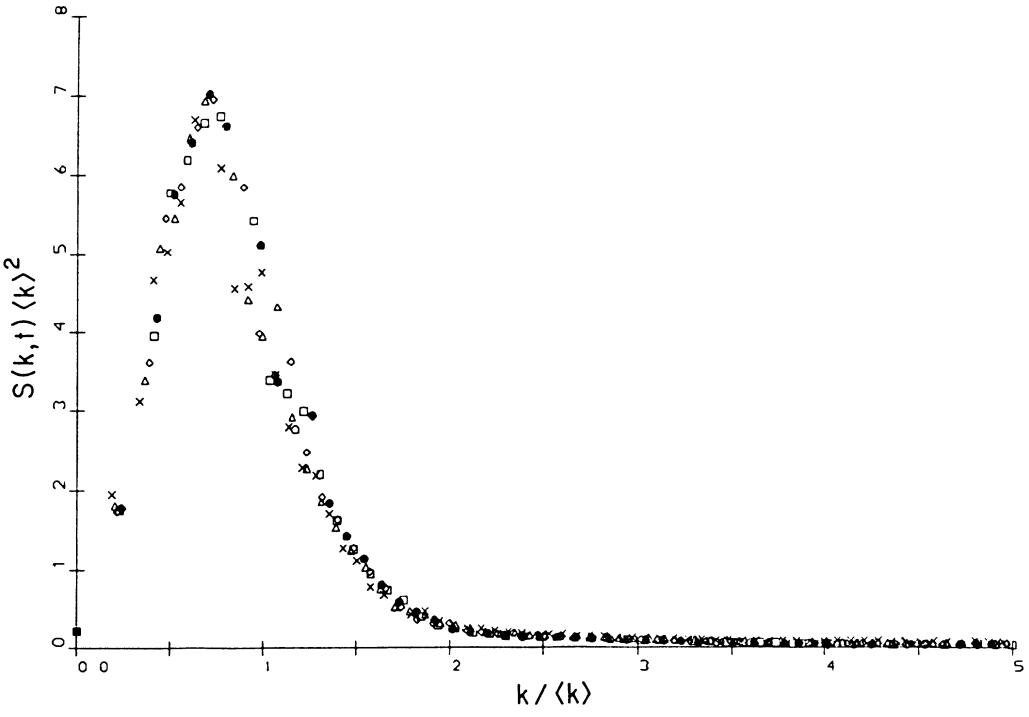

FIG. 19. Scaled form factors for the off-critically quenched (in the nucleation regime) conserved case of Fig. 18. Data from times 1200(×), 1600 (△), 2000 (◇), 2400 (□), and 2800 (●) are superposed. The master curve is quite different from that for the corresponding deterministic case.

Langer-Kitahara) equation. There is reason to believe this in the deeply quenched case (see Appendix). Preliminary results obtained in a simulation of a CDS version of the Langer (or Langer-Kitahara) equation by Yeung[23(c)] are very similar to the results obtained in the Monte Carlo simulation of Huse.[6(b)] There is still a possibility that the Monte Carlo results for Kawasaki exchange dynamics (in the very deep quench case) would give an asymptotic exponent of $\frac{1}{4}$ and not $\frac{1}{3}$. It seems that most existing numerical results can be made compatible with ours if we account for nonasymptoticity (shortness of simulations), freezing into metastable states, the delaying effect of noise, and the special features of Kawasaki exchange dynamics. The last point will be dealt with at length in a forthcoming paper.[23(c)]

ACKNOWLEDGMENTS

We are grateful to T. Ohta, H. Furukawa, and J. D. Gunton for many useful discussions and comments. We thank C. Yeung for his independent confirmation of our results and his critical reading of this manuscript. D. Jasnow pointed out that Eq. (A7) was originally proposed in the paper by Langer *et al.*[13(a)] We are grateful to M. Salamon for his interest in and generous support of our project. Our simulation was facilitated by V. Metze. This work was, in part, supported by National Science Foundation Grant. No. DMR-84-15063 through Materials Research Laboratory, University of Illinois at Urbana-Champaign, and by Grant No DMR-87-01393.

APPENDIX

In this Appendix we derive the interface kinetic equations as systematically as possible to make the involved mathematical difficulty explicit. We follow the treatment of Allen and Cahn[2b] (given in the context of the deterministic nonconserved case) to reduce the Cahn-Hilliard equation in the tubular neighborhood of the interface to

$$\frac{\partial\psi(\mathbf{r},t)}{\partial t}=-L\nabla^2[(\nabla\psi(\mathbf{r},t)\cdot\hat{\mathbf{n}}(\mathbf{r},t))\nabla\cdot\hat{\mathbf{n}}(\mathbf{r},t)]\ , \tag{A1}$$

where $\hat{\mathbf{n}}(\mathbf{r},t)$ is the unit vector locally normal to the interface. The interface position is defined through $\psi(\mathbf{r}_i(\mathbf{a},t),t)=0$. Introducing the Green's function $G(\mathbf{r},\mathbf{r}')$, where $\nabla^2G(\mathbf{r},\mathbf{r}')=-\delta(\mathbf{r}-\mathbf{r}')$ with appropriate boundary conditions, we can rewrite (A1) as

$$\int d\mathbf{r}'G(\mathbf{r},\mathbf{r})\frac{\partial\psi(\mathbf{r}',t)}{\partial t}=L[\nabla\psi(\mathbf{r},t)\cdot\hat{\mathbf{n}}(\mathbf{r},t)]\nabla\cdot\hat{\mathbf{n}}(\mathbf{r},t)\ . \tag{A2}$$

Since $\nabla\psi(\mathbf{r},t)\cdot\hat{\mathbf{n}}(\mathbf{r},t)=\partial\psi(n,t)/\partial n$ and is sharply peaked about $n=0$, we can integrate both sides of (A2) over n near the interface to get

$$\int dn\int d\mathbf{a}'\int dn'G(\mathbf{r}(\mathbf{a},n),\mathbf{r}')v(\mathbf{r}',t)\frac{\partial\psi(n'',t)}{\partial n''}\bigg|_{n''=n'}=2\psi_0LK(\mathbf{r}_i(\mathbf{a},t))\ , \tag{A3}$$

where K is the mean curvature (times spatial dimensionality) of the interface, the integration range for n and n' is an appropriate tubular neighborhood of the interface, and $v(\mathbf{r}',t)$ denotes the normal displacement velocity of the iso-ψ surface on which the point $\mathbf{r}'$ lies,

$$\frac{\partial\psi(\mathbf{r}_i(\mathbf{a},t),t)}{\partial t}=-\mathbf{v}(\mathbf{r}_i(\mathbf{a},t),t)\cdot\nabla\psi(\mathbf{r},t)\,|_{\,\mathbf{r}=\mathbf{r}_i(\mathbf{a},t)}\ . \tag{A4}$$

We can perform the integration over n' on the left-hand side of (A3) to cancel $2\psi_0$. This yields

$$\int dn\int d\mathbf{a}'G(\mathbf{r}(\mathbf{a},n),\mathbf{r}_i(\mathbf{a}',t))v(\mathbf{r}_i(\mathbf{a}',t))\ =LK(\mathbf{r}_i(\mathbf{a},t))\ , \tag{A5}$$

which is the required equation of motion for the conserved-order-parameter case (without noise). In the above derivation products of δ functions are avoided, but strictly speaking, it is still best to regard (A5) as a phenomenological equation which may be plausible in the thin wall limit. If the integration over n is appropriately approximated, (A5) reduces to the one originally derived by Kawasaki and Ohta.[12(a)]

In the CHC equation the Onsager kinetic coefficient L is a constant. The validity of this assumption must be carefully studied. The dependence of L on the order parameter has been discussed briefly by Langer *et al.*,[13(a)] who considered the following form:

$$L=L_0\{1-[\psi(\mathbf{r},t)/\psi_c]^2\}\ , \tag{A6}$$

where L_0 and ψ_c are positive constants. An equivalent form was also discussed by Kitahara and Imada.[23(a)] If we faithfully model Kawasaki exchange dynamics, the simplest continuum model has L of the above form.[23(b),23(c)] The diffusion of matter across bulk phases is considerably decelerated and the diffusion along the phase boundary becomes relatively more important. Thus there is a possibility that the CHC equation and the equation [which we would like to call the Langer (or Langer-Kitahara) equation]

$$\frac{\partial\psi(\mathbf{r},t)}{\partial t}=L_0\nabla\cdot\left\{\left[1-\left[\frac{\psi(\mathbf{r},t)}{\psi_c}\right]^2\right]\nabla\frac{\delta H[\psi(\mathbf{r},t)]}{\delta\psi(\mathbf{r},t)}\right\}+\sigma(\mathbf{r},t) \tag{A7}$$

may be in different universality classes. The parameter ψ_c plays a crucial role, however. If ψ_c is large compared to the equilibrium value ψ_0 (as a result of, say, vacancies), then (A7) virtually reduces to the CHC equation. In the

deep quenching case, diffusion through bulk phases becomes prohibitively difficult. In effect, the Langer (or Langer-Kitahata) equation takes the form

$$\frac{\partial\psi(\mathbf{r},t)}{\partial t}=L_{\|}\nabla_a^2\frac{\delta H[\psi(\mathbf{r},t)]}{\delta\psi(\mathbf{r},t)}\ , \tag{A8}$$

where $L_{\|}$ denotes the Onsager coefficient for diffusion along the interface and ∇_a^2 is the Laplacian on the interface with respect to the metric induced by the flat metric in the bulk. Proceeding as before, (A8) reduces to (on the interface)

$$-v(\mathbf{r}_i(\mathbf{a},t))\frac{\partial\psi(n,t)}{\partial n}\bigg|_{n=0}=-L_{\|}\nabla_a^2\left[\frac{\partial\psi(n,t)}{\partial n}\bigg|_{n=0}\nabla\cdot\hat{\mathbf{n}}(\mathbf{r},t)\bigg|_{\mathbf{r}=\mathbf{r}_i(\mathbf{a},t)}\right]\ , \tag{A9}$$

where all symbols have the same meaning as previously. But (by assumption)

$$\frac{\partial\psi(n,t)}{\partial n}\bigg|_{n=0}$$

varies only along the normal to the interface. Hence

$$\nabla_a^2\left[\frac{\partial\psi(n,t)}{\partial n}\bigg|_{n=0}\right]=0$$

and (A9) reduces to

$$v(\mathbf{r}_i(\mathbf{a},t))=L_{\|}\nabla_a^2K(\mathbf{r}_i(\mathbf{a},t))\ . \tag{A10}$$

Equation (A10) is the required interface equation which corresponds to the deeply quenched Langer (or Langer-Kitahara) equation. Equation (A7) and its CDS counterpart will be discussed in detail in a forthcoming paper.[23(c)]

If we apply dimensional analysis to interface equations we can get asymptotic exponents. Let l be the length scale of the pattern and τ be the time scale. The kinetic coefficient L does not depend on this length scale, so that we may regard it as dimensionless, viz., $[L]=1$. We have (notice that the integration near the interface with respect to n does not depend on l) $[\mathbf{a}]=l^{d-1}$, $[G]=l^{2-d}$, $[v]=l/\tau$, $[K]=1/l$. Replacing these in (A5) yields $l^{d-1}\times l^{2-d}\times l/\tau=1/l\Longrightarrow\tau\sim l^3$, so that $\phi=\frac{1}{3}$ for conserved dynamics. For the surface diffusion in the conserved case (without noise) described by (A10), we have $l/\tau=1/l^3\Longrightarrow\tau\sim l^4$, so that $\phi=\frac{1}{4}$. This exponent is possible asymptotically only when there is strictly no diffusion through the bulk phase; if there is a small bulk diffusion, the exponent will eventually crossover from $\frac{1}{4}$ to $\frac{1}{3}$.

[1]For reviews, see J. D. Gunton, M. San Miguel, and P. S. Saint, in *Phase Transitions and Critical Phenonema,* edited by C. Domb and J. L. Lebowitz (Academic, New York, 1983), Vol. 8; J. L. Lebowitz, J. Marro, and M. H. Kalos, Comments Solid State Phys. **10**, 201 (1983); H. Furukawa, Adv. Phys. **34**, 703 (1985); K. Binder, in *Statistical Physics,* edited by H. E. Stanley (North-Holland, Amsterdam, 1986); J. D. Gunton (unpublished).

[2](a) M. T. Collins and H. C. Teh, Phys. Rev. Lett. **30**, 781 (1973); D. G. Morris, F. M. Besag, and R. E. Smallman, Philos. Mag. **29**, 43 (1974); T. Hashimoto, K. Nishihara, and Y. Takeuchi, J. Phys. Soc. Jpn. **45**, 1127 (1978); (b) S. M. Allen and J. W. Cahn, Acta Metall. **27**, 1085 (1979); (c) Y. Noda, S. Nishihara, and Y. Yamada, J. Phys. Soc. Jpn. **53**, 4241 (1984).

[3](a) A. F. Craievich and J. M. Sanchez, Phys. Rev. Lett. **47**, 1308 (1981); A. F. Craievich, J. M. Sanchez, and C. E. Williams, Phys. Rev. B **34**, 2762 (1986); M. Hennion, D. Ronzaud, and P. Guyot, Acta Metall. **30**, 599 (1982); S. Katano and M. Iizumi, Phys. Rev. Lett. **52**, 835 (1984); (b) B. D. Gaulin, S. Spooner, and Y. Morii, Phys. Rev. Lett. **59**, 668 (1987).

[4]M. K. Phani, J. L. Lebowitz, M. H. Kalos, and O. Penrose, Phys. Rev. Lett. **45**, 366 (1980); P. S. Sahni, G. Dee, J. D. Gunton, M. Phani, J. L. Lebowitz, and M. H. Kalos, Phys. Rev. B **24**, 410 (1981); E. T. Gawlinski, M. Grant, J. D. Gunton, and K. Kaski, *ibid.* **31**, 281 (1985); G. F. Mazenko and O. T. Valls, *ibid.* **27**, 6811 (1983); F. C. Zhang, O. T. Valls, and G. F. Mazenko, *ibid.* **31**, 1579 (1985); G. S. Grest and D. J. Srolovitz, *ibid.* **30**, 5150 (1984).

[5]J. Marro, J. L. Lebowitz, and M. H. Kalos, Phys. Rev. Lett. **43**, 282 (1979); O. Penrose, J. L. Lebowitz, J. Marro, M. H. Kalos, and A. Sur. J. Stat. Phys. **19**, 243 (1978); J. L. Lebowitz, J. Marro and M. H. Kalos, Acta Metall. **30**, 297 (1982); P. S. Sahni and J. D. Gunton, Phys. Rev. Lett. **45**, 369 (1980); see also G. S. Grest and D. J. Srolovitz, Phys. Rev. B **30**, 5150 (1984).

[6](a) G. F. Mazenko, O. T. Valls, and F. C. Zhang, Phys. Rev. B **32**, 5807 (1985); (b) D. Huse, Phys. Rev. B **34**, 7845 (1986); after the submission of this paper, extensive Monte Carlo simulation results were published by J. G. Amar, F. E. Sullivan, and R. D. Mountain, Phys. Rev. B **37**, 196 (1988). Their asymptotic form factor is less sharp than our asymptotic functional form. We are not sure whether their model and the models used in the ordinary Monte Carlo simulations are the same; (c) G. F. Mazenko and O. T. Valls, Phys. Rev. Lett. **59**, 680 (1987).

[7](a) R. Petschek and H. Metiu, J. Chem. Phys. **79**, 3443 (1985); (b) T. Miyazaki, T. Kozakai, S. Mizuno, and M. Doi, Trans. Jpn. Inst. Met. **24**, 799 (1983); (c) E. T. Gawlinski, J. D. Gunton, and J. Vinãls (unpublished); (d) P. Meakin, H. Metiu, R. G. Petschek, and D. J. Scalapino, J. Chem. Phys. **79**, 1948 (1983).

[8]A. Chakrabarti and J. D. Gunton, Phys. Rev. B **37**, 3798 (1988).

[9]J. W. Cahn and J. E. Hilliard, J. Chem. Phys. **28**, 258 (1958); I.

M. Lifshitz and V. V. Slyozov, J. Phys. Chem. Solids **19**, 35 (1961); H. E. Cook, Acta Metall. **18**, 297 (1970).

[10](a) K. Binder and D. Stauffer, Phys. Rev. Lett. **33**, 1006 (1974); (b) H. Furukawa, Phys. Lett. **62A**, 377 (1977); Prog. Theor. Phys. **59**, 1072 (1978); Phys. Rev. Lett. **43**, 136 (1979); Phys. Rev. A **23**, 1535 (1981); see also his review article cited in Ref. 1.

[11](a) K. Kawasaki, M. C. Yalabik, and J. D. Gunton, Phys. Rev. A **17**, 455 (1978); (b) T. Ohta, D. Jasnow, and K. Kawasaki, Phys. Rev. Lett. **49**, 1223 (1982).

[12](a) K. Kawasaki and T. Ohta, Prog. Theor. Phys. **67**, 147 (1982); **68**, 129 (1982); K. Kawasaki, Butsuri **38**, 919 (1983); Ann. Phys. **154**, 319 (1984); K. Kawasaki and T. Ohta, Prog. Theor. Phys. **67**, 147 (1982); Physica A **118**, 175 (1983); (b) K. Kawasaki, Y. Enomoto, and M. Tokuyama, Physica A **135**, 426 (1986); M. Tokuyama, Y. Enomoto, and K. Kawasaki, *ibid.* **143**, 183 (1987); (c) T. Ohta, Prog. Theor. Phys. Suppl. **71**, 1409 (1984); Ann. Phys. **158**, 31 (1984).

[13](a) J. S. Langer, M. Bar-On, and H. P. Miller, Phys. Rev. A **11**, 1417 (1975); (b) K. Binder, Phys. Rev. B **15**, 4425 (1977); (c) C. Billotet and K. Binder, Z. Phys. B **32**, 195 (1979); K. Binder, Phys. Rev. B **15**, 4143 (1977).

[14]Y. Oono and S. Puri, Phys. Rev. A **38**, 434 (1988).

[15]Y. Oono and S. Puri, Phys. Rev. Lett. **58**, 836 (1987); see also Y. Oono and Y. Shiwa, Mod. Phys. Lett. B **1**, 49 (1987).

[16](a) For example, see S. Wolfram, *Theory and Applications of Cellular Automata* (World Scientific, Singapore, 1986); J. Demongeot, E. Cole, and M. Tchuente, *Dynamical Systems and Cellular Automata* (Academic, New York, 1985); (b) K. Kaneko, Prog. Theor. Phys. **72**, 480 (1984); R. J. Deissler, Phys. Lett. **100A**, 451 (1984); R. Kapral, Phys. Rev. A **32**, 1076 (1985); (c) G. L. Oppo and R. Kapral, Phys. Rev. A **33**, 4219 (1986); R. Kapral and G. L. Oppo, Physica D **23**, 455 (1986); G. L. Oppo and R. Kapral (unpublished).

[17]U. Frisch, B. Hasslacher, and Y. Pomeau, Phys. Rev. Lett. **56**, 1505 (1986); S. Orszag and V. Yakhot, *ibid.* **56**, 1691 (1986); H. Chen and W. H. Matthaeus, *ibid.* **58**, 1845 (1987).

[18]J. Greenberg, C. Green, and S. Hastings, SIAM (Soc. Ind. Appl. Math.) J. Algebraic Discrete Methods **1**, 34 (1980); B. F. Madore and W. L. Freedman, Science **222**, 615 (1983); D. A. Young, Math. Biosci. **72**, 51 (1984); Y. Oono and M. Kohmoto, Phys. Rev. Lett. **55**, 2927 (1985); Y. Oono and C. Yeung, J. Stat. Phys. **48**, 593 (1987).

[19]T. Ohta (private communication); also see Ref. 11(b).

[20]Y. Oono, S. Puri, C. Yeung, and M. Bahiana, J. Appl. Crystallogr. (to be published); S. Puri and Y. Oono, J. Phys. A (to be published).

[21](a) H. Tomita, Prog. Theor. Phys. **72**, 656 (1984); **75**, 482 (1986); (b) G. Porod, in *Small Angle X-Ray Scattering,* edited by O. Glatter and L. Kratky (Academic, New York, 1983); (c) Y. Oono and S. Puri, Mod. Phys. Lett. B (to be published).

[22]C. Yeung (private communication).

[23](a) K. Kitahara and M. Imada, Prog. Theor. Phys. Suppl. **64**, 65 (1978); (b) K. Kitahara, Y. Oono, and D. Jasnow, Mod. Phys. Lett. B (to be published); T. Ohta, J. Phys. C (to be published); (c) C. Yeung and Y. Oono (unpublished).

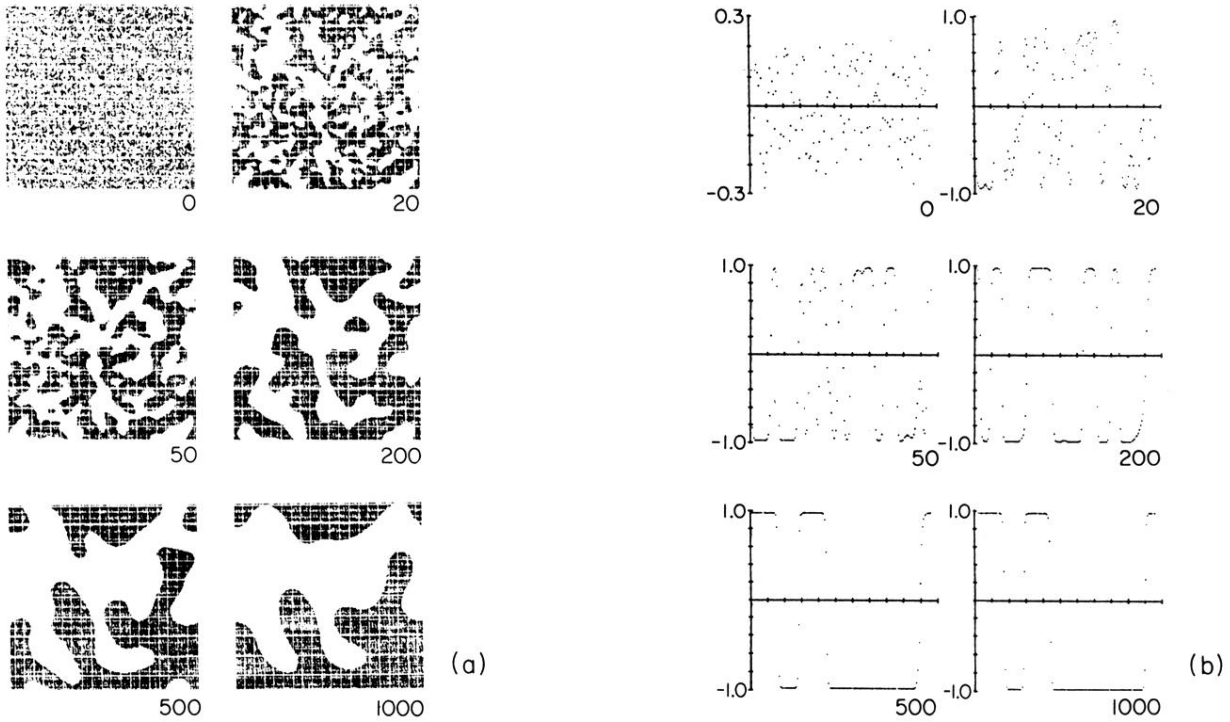

FIG. 1. (a) Evolution pattern for the nonconserved case (without noise) for a 150×150 lattice. The initial configuration (labeled by 0) has order-parameter values uniformly and randomly distributed between ±0.125. The numbers denote necessary time steps from the initial condition. Only points with positive order parameter are marked. This coding is also used in all subsequent evolution patterns we display in this paper. (b) Evolution of the domain-wall structure for the situation shown in (a). The figures correspond to the variation of the order parameter along the diagonal from $(n_x=1,n_y=1)$ to $(n_x=150,n_y=150)$; the segment between adjacent horizontal tick marks corresponds to about 14 diagonal lattice elements. The numbers along the vertical axes denote the order-parameter values. Again, the integers denote the number of time steps from the initial condition. Well-defined walls (about 1–2 sites thick) are formed by about 50 updates.

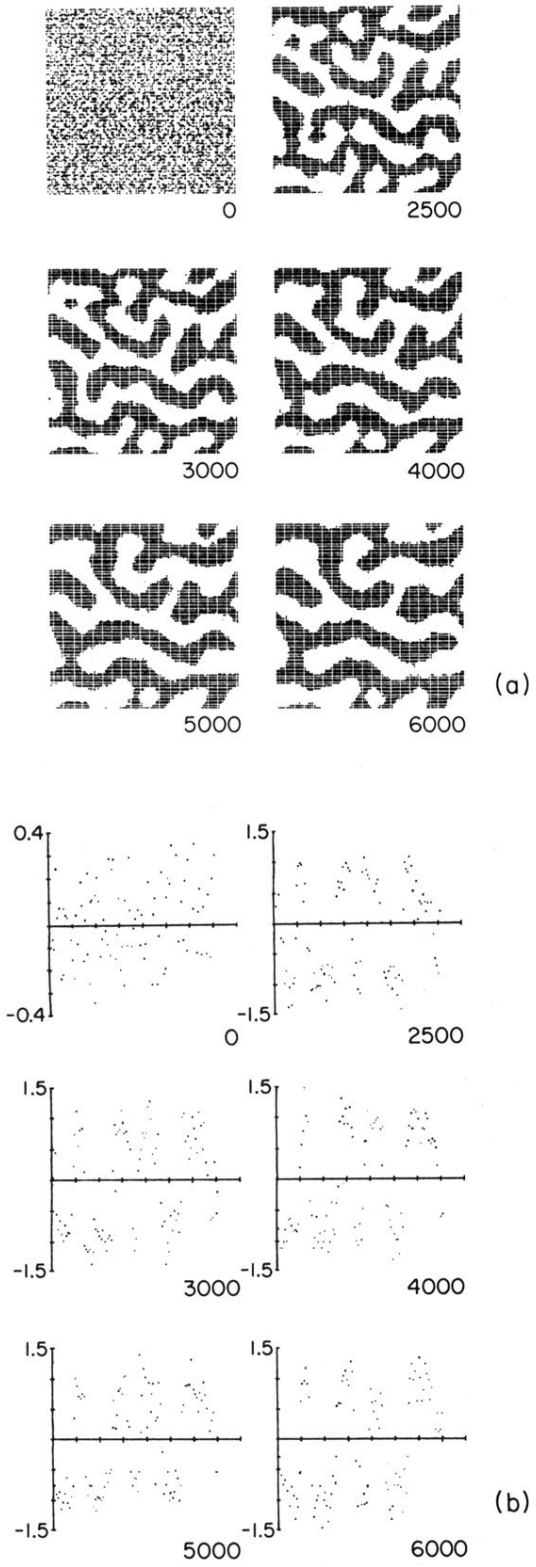

FIG. 10. (a) Evolution pattern for the conserved case (with noise $B=0.3$) with a critical quench for a 100×100 lattice. The integers denote necessary updates. The initial configuration is the same as in Fig. 7(a). (b) Evolution of the domain-wall structure for the situation shown in (a). For the numbers and tick marks in the figure see the legend for Fig. 7(b). The section is the same as in Fig. 7(b). As pointed out in the text, the noise amplitude used is unrealistically large and the domains are not well formed.

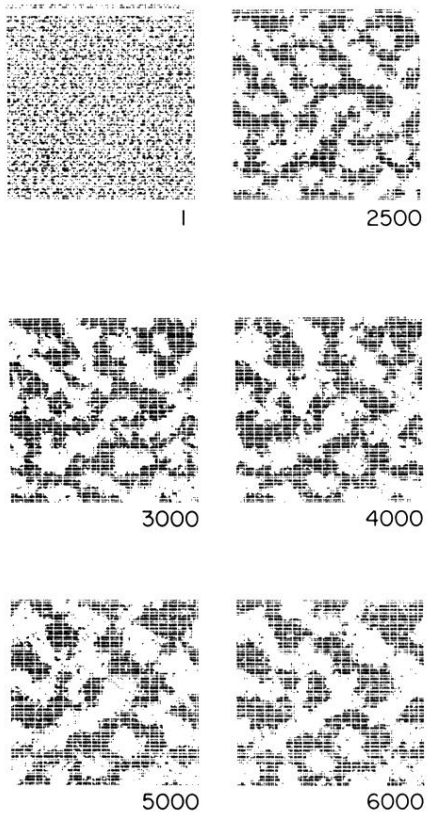

FIG. 11. Evolution pattern for the critically quenched conserved case with "strong" noise $B=0.5$ for a 100×100 lattice. The integers denote necessary updates. Once again, the initial configuration is the same as in Fig. 7(a). The pattern is similar to previously published patterns from Monte Carlo simulations [Refs. 5 and 6(b)] or Langevin simulations of the CHC equation (Ref. 7).

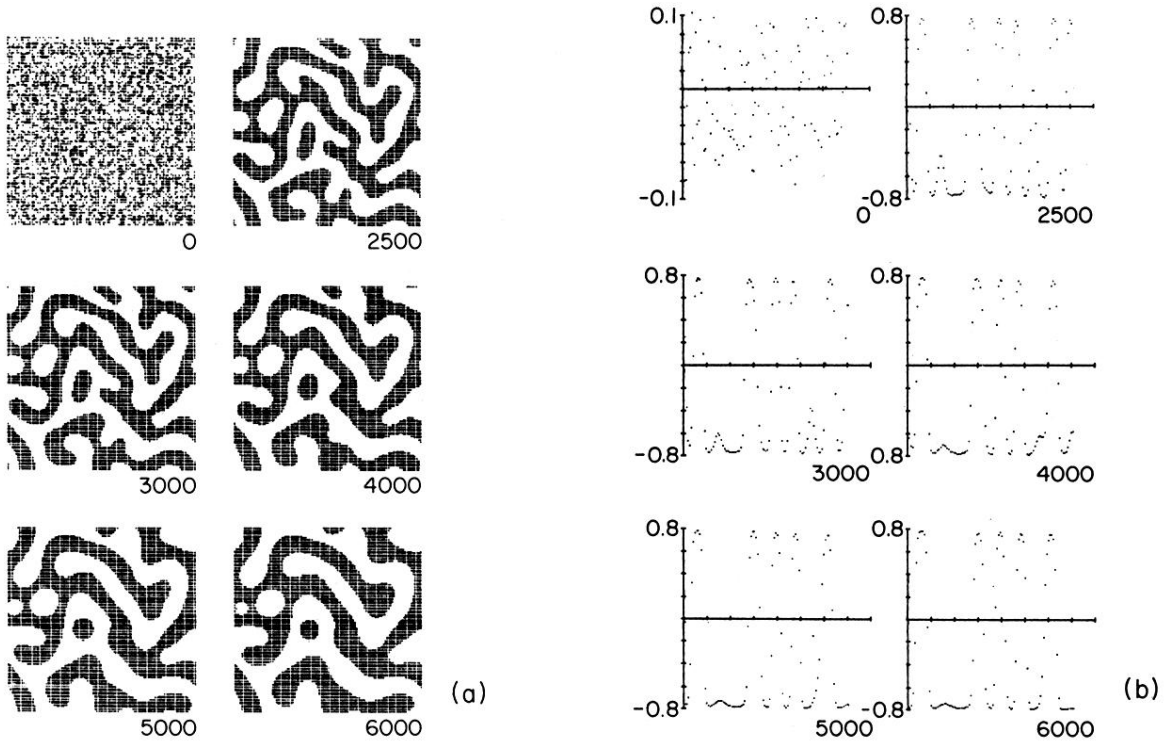

FIG. 14. (a) Evolution pattern for the "soft-wall" conserved case (without noise) with a critical quench for a 100×100 lattice. The integers denote necessary updates. The parameters used are $A=1.2$ and $D=0.5$. The initial configuration is the same as in Fig. 7(a). (b) Evolution of the domain-wall structure for the situation shown in (a). For the numbers and tick marks see the legend for Fig. 7(b). The section is the same as in Fig. 7(b). The domain walls are somewhat softer than those in Fig. 7(b).

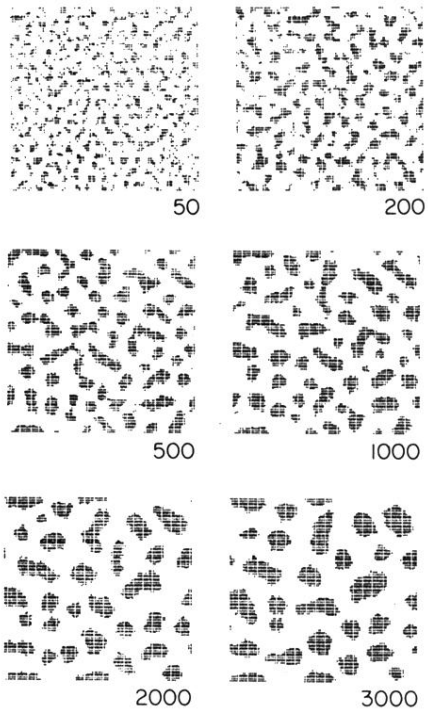

FIG. 16. Evolution pattern for the off-critically quenched conserved case (with noise $B=0.3$) for a 100×100 lattice. The initial configuration corresponds to the order parameter at the sites being randomly and uniformly distributed between -0.3 ± 0.125.

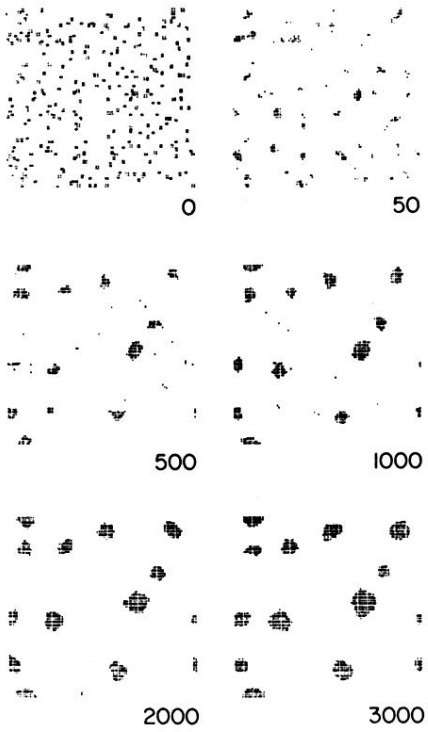

FIG. 18. Evolution pattern for the off-critically quenched conserved case (with noise $B=0.3$) with quenching in the nucleation regime. The integers denote necessary updates. Again, the lattice size is 100×100. For the initial configuration see the text.

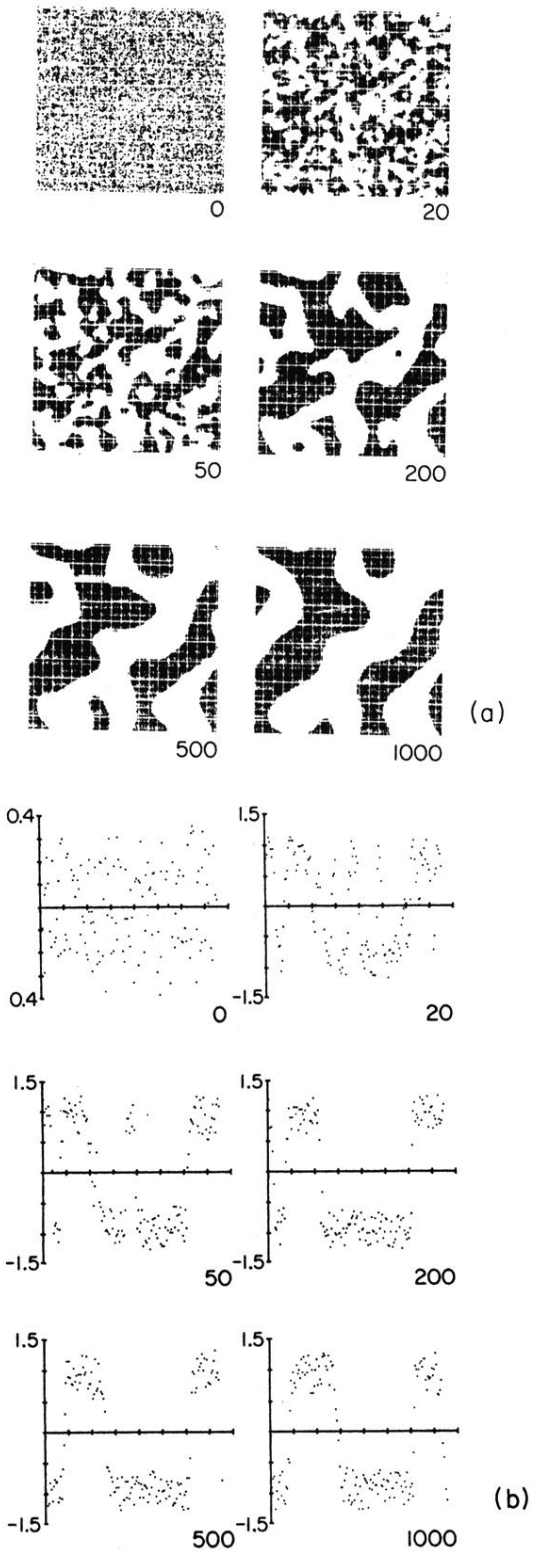

FIG. 5. (a) Evolution pattern for the nonconserved case with noise $B=0.3$ for a 150 lattice. The initial configuration is the same as in Fig. 1(a). The domain boundaries are somewhat more ragged than those of the deterministic case. (b) Evolution of the domain-wall structure for the situation shown in (a). However, this time the section is along the horizontal line in the middle. For numbers see the legend for Fig. 1(a). The segment between adjacent horizontal tick marks corresponds to about 14 lattices. The noise amplitude used is unrealistically large and the domains are not very well formed.

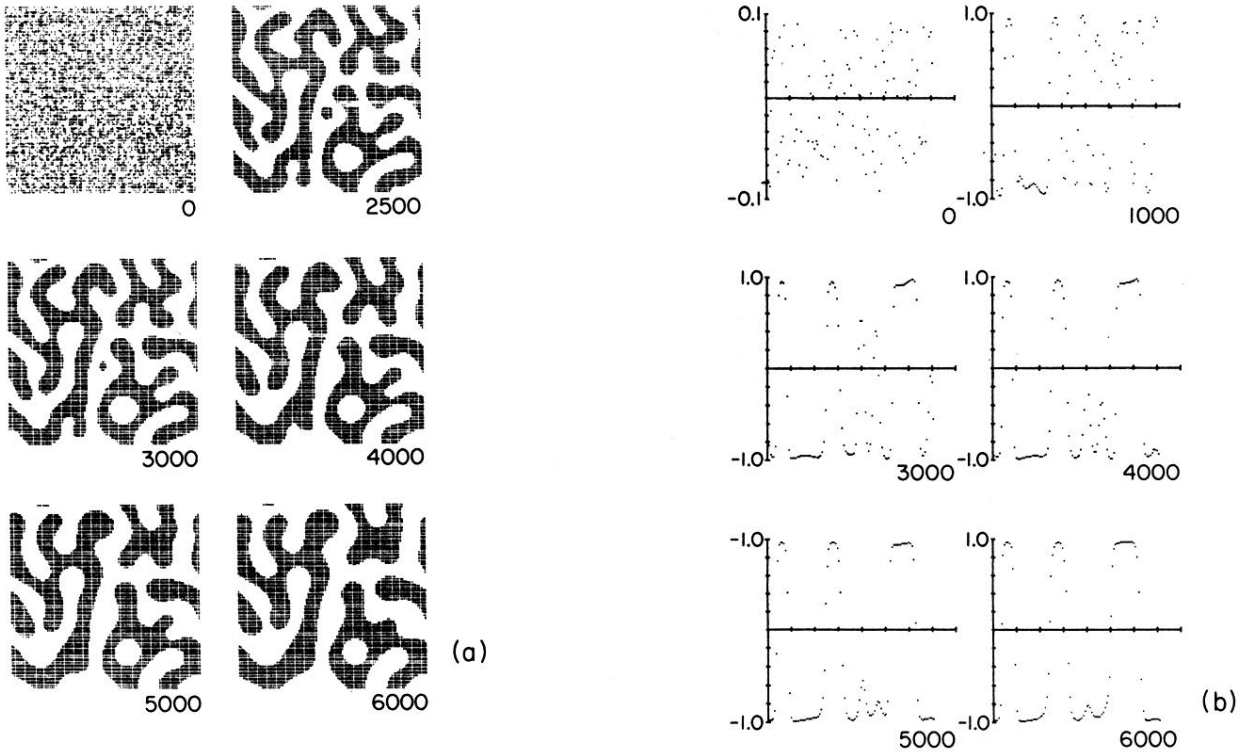

FIG. 7. (a) Evolution pattern for the conserved case (without noise) with a critical quench for a 100×100 lattice. The integers denote necessary updates. The initial configuration consists of order-parameter values randomly and uniformly distributed between ±0.125 as in Fig. 1(a). Of course, this corresponds to a different initial condition because of the different sizes of the lattices. (b) Evolution of the domain-wall structure for the situation shown in (a). The numbers along the vertical axes denote the order-parameter values, and the interval between the adjacent tick marks corresponds to about 13 lattice spacings. The times are the same as those in (a) except for the figure in the upper-right corner. It is taken at 1000 updates and indicates that well-formed domains appear by that time. The section is along the diagonal form $(n_x=1,n_y=1)$ to $(n_x=100,n_y=100)$, as in Fig. 5(a).